PL-TR-92-2218(II)

TEST AND EVALUATION OF NEURAL NETWORK APPLICATIONS FOR SEISMIC SIGNAL DISCRIMINATION

Gagan B. Patnaik
Thomas J. Sereno, Jr.
Richard D. Jenkins

Science Applications International Corporation
10260 Campus Point Drive
San Diego, California 92121

28 September 1992

Final Report (Volume II)
1 September 1990 – 31 August 1992

PHILLIPS LABORATORY
Directorate of Geophysics
AIR FORCE MATERIEL COMMAND
HANSCOM AIR FORCE BASE, MA 01731-5000

The views and conclusions contained in this document are those of the authors and should not be interpreted as representing the official policies, either expressed or implied, of the Air Force or the U.S. Government.

This technical report has been reviewed and is approved for publication.

JAMES F. LEWKOWICZ
Contract Manager
Solid Earth Geophysics Branch
Earth Sciences Division

JAMES F. LEWKOWICZ
Branch Chief
Solid Earth Geophysics Branch
Earth Sciencs Division

DONALD H. ECKHARDT, Director
Earth Sciences Division

This document has been reviewed by the ESD Public Affairs Office (PA) and is releasable to the National Technical Information Service (NTIS).

Qualified requestors may obtain additional copies from the Defense Technical Information Center. All others should apply to the National Technical Information Service.

If your address has changed, or if you wish to be removed from the mailing list, or if the addressee is no longer employed by your organization, please notify PL/IMA, Hanscom AFB MA 01731-5000. This will assist us in maintaining a current mailing list.

Do not return copies of this report unless contractual obligations or notices on a specific document requires that it be returned.

REPORT DOCUMENTATION PAGE

Form Approved
OMB No. 0704-0188

1 AGENCY USE ONLY (Leave blank)	2 REPORT DATE	3 REPORT TYPE AND DATES COVERED
	28 September 1992	Final Report (Volume II) 9/1/90-8/31/92

4 TITLE AND SUBTITLE
Test and Evaluation of Neural Network Applications for Seismic Signal Discrimination

5 FUNDING NUMBERS
PE 61101E
PR 9T10 TA DA WU AA
Contract F19628-90-C-0156

6 AUTHOR(S)
Gagan B. Patnaik, Thomas J. Sereno, Jr., Richard D. Jenkins

7 PERFORMING ORGANIZATION NAME(S) AND ADDRESS(ES)
Science Applications Intern'l Corp
10260 Campus Point Drive
San Diego, CA 92121

8 PERFORMING ORGANIZATION REPORT NUMBER
SAIC-92/1191

9 SPONSORING/MONITORING AGENCY NAME(S) AND ADDRESS(ES)
Phillips Laboratory
Hanscom AFB, MA 01731-5000

Contract Manager: James Lewkowicz/GPEH

10 SPONSORING/MONITORING AGENCY REPORT NUMBER
PL-TR-92-2218 (II)

11 SUPPLEMENTARY NOTES

12a DISTRIBUTION/AVAILABILITY STATEMENT
Approved for public release; Distribution unlimited

12b DISTRIBUTION CODE

13 ABSTRACT *(Maximum 200 words)*

This report describes operational test and evaluation of two neural network applications that were integrated into the *Intelligent Monitoring System (IMS)* for automated processing and interpretation of regional seismic data. Also reported is the result of a preliminary study on the application of neural networks to regional seismic event identification. The first application is for initial identification of seismic phases (*P* or *S*) recorded by 3-component stations based on polarization data and context. This neural network performed 3-6% better than the current rule-based system when tested on data obtained from the 3-component IRIS stations in the former Soviet Union. This resulted in an improved event bulletin which showed that the number of analyst-verified events that were missed by the automated processing decreased by more than a factor of 2 (about 10 events/week). The second operational test was conducted on the neural network developed by MIT/Lincoln Laboratory for regional final phase identification (e.g., *Pn*, *Pg*, *Sn*, *Lg*, and *Rg*). This neural network performed 3.3% better than the rule-based system in *IMS* station processing. However, for the final phase identifications obtained after network processing (where data from all stations are combined), the gain dropped to about 1.0%. It is likely that this could be regained by using the neural network phase identification confidence factors in the network processing. Finally, our preliminary study on the application of neural networks to identify regional seismic events on the basis of *coda* shape gave about 80% accuracy on data recorded at GERESS. In general, the neural network classifier utilized the *coda* decay rate which was lower for the earthquakes than it was for the explosions, although there was substantial overlap.

14 SUBJECT TERMS	15 NUMBER OF PAGES
Neural Networks, Seismic Signal Discrimination, Test and Evaluation, Phase ID, Event ID	62
	16 PRICE CODE

17 SECURITY CLASSIFICATION OF REPORT	18 SECURITY CLASSIFICATION OF THIS PAGE	19 SECURITY CLASSIFICATION OF ABSTRACT	20 LIMITATION OF ABSTRACT
Unclassified	Unclassified	Unclassified	SAR

Table of Contents

1. OVERVIEW

1.1 Objectives

The objectives of this two-year project were:

- *Assemble data sets to be used to test and evaluate the performance of neural networks for automated processing and interpretation of seismic data.*

- *Evaluate the results of the neural network applications in the context of monitoring nuclear explosion testing.*

One of the goals of DARPA's Artificial Neural Network Technology (*ANNT*) program is to determine whether or not neural networks can improve upon current methods for seismic monitoring of underground nuclear explosion testing. DARPA's Intelligent Monitoring System (*IMS*) is a prototype surveillance system for developing and demonstrating new technology for regional monitoring of small or clandestine underground nuclear tests. Therefore, to meet the goal of the *ANNT* program, the neural network technology applications were targeted for specialized processing tasks of *IMS*. Our first objective was to build relevant data sets to be used to test and evaluate the performance of the neural networks. These data were recorded by the high-frequency arrays used in *IMS*. The work performed to achieve this objective is described in detail in Volume I of our annual report [*Sereno and Patnaik*, 1991] and in Volume I of this final report [*Sereno, et al.*, 1992]. These data were to be used to develop and train neural networks to perform specialized seismic data processing and interpretation tasks (e.g. automated phase identification, onset time estimation, phase association, typical and atypical event recognition, and event identification), and to test the generality and adaptability of neural networks.

To achieve our second objective, we integrated two neural network modules into the *IMS*, and tested them under simulated operational conditions. One of these was developed by MIT/Lincoln Laboratory for regional seismic phase identification (e.g., *Pn, Pg, Sn, Lg, Rg*). This module is described by *Lacoss, et al.* [1990]. We developed the other neural network module which performs initial seismic phase identification (*P* or *S*) from 3-component seismic data. This is described in Volume II of our annual report [*Patnaik and Sereno*, 1991]. This final report (Volume II) describes the results of our simulated operational testing. In particular, we report on the improvement in the final event bulletin that is obtained by using neural networks for automated seismic phase identification. Also included are the design and preliminary results of a neural network technique for identifying regional seismic events on the basis of *coda* shape.

1.2 Summary of Neural Network Applications

1.2.1 Initial Phase Identification

An initial phase identification (*P* or *S*) neural network module was developed based on polarization and context data from 3-component stations, and it was implemented in *IMS* [*Patnaik and Sereno*, 1991]. For operational testing and evaluation, the *IMS* was applied to a 6-week period of continuous data from the IRIS/IDA stations in the former Soviet Union [*Swanger, et al*, 1992]. This test was done twice; once with the rule-based method for initial phase identification, and once using the trained neural networks. The neural networks performed 3-6% better than the current *IMS* rules, and the improvement was greater for *P*-phases than it was for *S*-phases (about 67% of the detections in the test data set were *P*-phases). Although this technique works best for site-specific applications, so far we have only trained separate neural networks for the stations AAK and GAR. We did not have enough analyst-reviewed data from the stations OBN, TLY, ARU, and KIV to develop stable station-specific neural network weights. Therefore, for these stations we used average weights that were derived from data recorded by all 6 IRIS/IDA stations.

The improvement realized in the phase identification accuracy also had a significant impact on the final automated bulletin (particularly on the number of events missed by the automated processing). The analyst accepted more of the events formed by the automated system when the neural network was used for initial phase identification, and fewer events were missed by the automated processing. For example, approximately 10 more analyst-verified events per week were formed when the neural network was used for initial phase identification than when the current *IMS* rule-based system was used. Larger gains are expected once enough data are available at all IRIS/IDA stations to derive a full set of station-specific weights. Also, the analysis procedures only included events recorded at ≥2 stations, so the test database is biased towards high *snr* data from the stations AAK and GAR (92% of the test data have *snr* >2). The improvement offered by the neural networks is greater for the other stations, so larger gains should be seen for routine analysis of data from all stations.

The key advantages of the neural network approach to automated initial identification of seismic phases recorded by 3-component stations are:

- *Better performance than competing technologies.* The neural network consistently performed 3-6% better than both the current *IMS* rule-based system, and a linear multi-variate statistical technique [*Patnaik and Sereno*, 1991].

- *Extensibility.* The neural network approach is easily extended to include new features, which could be extremely difficult for a conventional rule-based system.

- *Adaptability.* The neural network is easily adapted to data from new stations. For example, the identification accuracy (*P* or *S*) is 75-85% without retraining (*e.g.*, using weights derived with data from a different station), and it is typically >95% after retraining with data from the same station. Enough data can be accumulated for retraining within a few weeks of continuous station operation, and training takes <30 minutes on a Sun Sparc Station.

- *Amenable to automated learning techniques.* The neural network approach is easily adapted to automated learning (e.g., training).

1.2.2 Regional Phase Identification (MIT/Lincoln Lab)

MIT/Lincoln Laboratory's neural network module for regional phase identification was integrated in *IMS*, and was tested under operational conditions. We applied *IMS* with and without the neural network to data recorded by the four European regional arrays (ARCESS, NORESS, FINESA, and GERESS) during April, 1991. The results of each run were compared to the analyst-reviewed solutions to estimate identification accuracy of the neural networks.

The neural networks performed about 3.3% better than the rule-based component in *IMS* for station processing. Much of this performance gain is due to more accurate identification of *Sn*. However, after network processing (where data from all stations are combined), the gain of the neural network drops to about 1.0%. Therefore, the final event bulletin produced using the neural network in station processing is not much different than the bulletin produced by the original rule-based system. For example, 95% of the 2142 events formed using the neural network are identical to events formed with the rule-based system. The neural network did only slightly better than the rule-based system on the 5% that were different. However, it is possible that higher gains could be realized if network processing rules were improved (by incorporating the phase identification confidence measures produced by the neural network).

1.2.3 Regional Event Identification

A preliminary study involving a neural network technique for the identification of regional events on the basis of broad-band envelope shape was carried out with 61 regional events recorded at GERESS. Close to perfect separation between earthquakes and explosions could be achieved if both P and S envelopes were used. However, this may be caused by propagation effects, rather than source differences. For example, all of the earthquakes were to the south of the Alps, and these have small Lg phases (probably due to structural blockage) relative to the mining explosions to the north of GERESS. Using only *P-coda* envelopes, in the group velocity range 6.0–5.0 km/s, close to 80% identification accuracy was obtained for the data set. In general, the coda decay rate is lower for the earthquakes than it is for the explosions, although there is much overlap. The neural network classifier utilized this difference in decay rate for classifying the events.

1.3 Outline of the Report

This final report is divided into two volumes. Volume I is a description of Data Sets #2–3 [*Sereno, et al.*, 1992]. This report is Volume II of our final report. Section 2 presents the results of operational testing and evaluation of our initial phase identification (*P* or *S*) neural network module. Section 3 describes the results obtained from the operational testing of the regional phase identification (e.g., *Pn*, *Pg*, *Sn Lg*, *Rg*) neural network module developed by MIT/Lincoln Laboratory. Section 4 describes our study on regional event identification from GERESS recordings. Our conclusions regarding these neural network applications to automated interpretation of regional seismic data are presented in Section 5.

2. INITIAL PHASE ID NEURAL NETWORK MODULE

A neural network module was developed for automated initial identification of seismic phases (*P* or *S*) based on polarization and context data from 3-component stations, and it was implemented in *IMS*. Details of the design, development and application of the neural network technique are presented in Volume II of our annual report [*Patnaik and Sereno*, 1991]. Brief descriptions of the development of this technique, the results, and a comparison with the multivariate discriminant approach are reproduced in this final report. However, most of this section describes new results obtained with the 3-component data from 6 IRIS/IDA stations in the former Soviet Union, and the results obtained under operational testing of the neural network module.

2.1 Neural Network Development

2.1.1 Technique

In *IMS* station processing initial phase identification is done differently for array stations and for single 3-component stations. For the array stations, the apparent phase velocity (estimated from a broad-band F–K analysis) is used to separate detections into Teleseism, Regional P, Regional S, or Noise [*Bache, et al.*, 1990; *Bache, et al.*, 1992]. In this case the identification is nearly perfect between *P*- and *S*-type phases. However, accurate estimates of phase velocity are not available for 3-component data. Instead, automated phase identification is based on a combination of polarization data and context using neural networks as pattern matchers [*Patnaik and Sereno*, 1991]. A vector consisting of polarization and context data is treated as a pattern corresponding to an analyst-identified phase (*ground truth*). A neural network is then designed and trained using these patterns. Separate data sets are used for training and testing, so that a well-generalized set of weights is obtained. Neural network parameters (like the number of nodes in the middle layer) are problem-dependent and are estimated empirically. The derived neural network weights are station-dependent. That is, site-specific characteristics are developed by deriving separate weights for each station. In addition, an empirically estimated confidence factor is provided for each phase identification by the neural network.

2.1.2 Results

This neural network technique was initially tested by applying it to 3-component data from the four high-frequency arrays (ARCESS, NORESS, FINESA, and GERESS), a single 3-component stations in Ksiaz, Poland (KSP), and a 3-component broad-band station in Garm (GAR), former Soviet Union. Neural networks performed better than the current rule-based system in *IMS*, and better than a linear multivariate technique applied to the same data (see the next section). The biggest improvement was for signals with low *snr*. The percentage of correct identification for ARCESS and NORESS was 92–99% for data with 3-component $snr > 2$ and 86–96% for all *snr*. We also applied this technique to data from each of the 3-component elements of the

NORESS and ARCESS arrays. Site-dependence was observed among these 3-component array elements, and the identification accuracy varied from 80–92%. We found that the networks trained with NORESS/ARCESS data achieved about 80% identification accuracy when tested with data recorded at GAR. After retraining with data from GAR, the accuracy increased by 10–15%. These reported results were based on polarization data alone. We have since added *context* (e.g., relative number of arrivals surrounding a detection and their relative arrival times) to the neural networks and the results are typically 3–4% higher.

2.1.3 Comparative Study

There are several competing techniques that can be applied to the problem of automated initial phase identification. In addition to the back-propagation neural network approach, we applied the *Learning Vector Quantization (LVQ)* method to a test data set from ARCESS and NORESS. The identification accuracy was 5–8% lower. *Suteau-Henson* [1992*a*] and *Riviere-Barbier, et al.* [1992] reported automated initial phase identification from polarization data (without context) for 3-component IRIS/IDA stations. They used a multivariate discriminant analysis method to identify regional and teleseismic *P*-type and *S*-type phases. Their identification accuracy was slightly lower than the results of our neural network method reported here. Recently, *Suteau-Henson*, [1992*a*] expanded her multivariate discriminant method to incorporate "noise" detections as a separate class. She reports an average identification accuracy of about 75%. As expected, it was difficult to separate teleseisms from regional P phases, and regional S phases from noise. We have not tried a similar experiment with the neural network approach. However, we have done a direct performance comparison between the neural network method and the multivariate discriminant analysis method on a common set of NORESS and ARCESS data. The results indicated 3-7% higher accuracy by the neural network method [*Patnaik and Sereno*, 1991]. *Suteau-Henson* [1992*b*] expanded on this by comparing the neural network and multivariate confidence estimates for cases where either method failed. She found that there is not much overlap in the failed sets, so it is possible that a combination of the two methods could improve the overall phase identification accuracy (the confidence estimates would be used to resolve conflicts).

2.1.4 Implementation in IMS

A software module was developed for automated initial identification of seismic phases (*P* or *S*) based on our neural network technique. This module was implemented into a test version of the *Expert System for Association and Location* (ESAL) which is a knowledge-based component of *IMS* [*Bratt, et al.*, 1991; *Bache, et al.*, 1992]. The implementation is shown schematically in Figure 1. The signal processing component of *IMS* performs detection and feature extraction (arrival time, frequency, amplitude, polarization parameters, etc). Only a few of these attributes are used by the current rule-based system to identify each detection as a *P*-wave or as an *S*-wave from 3-component stations. This process is called *initial phase identification* in Figure 1. This is where the rule-based method has been replaced by the neural network method.

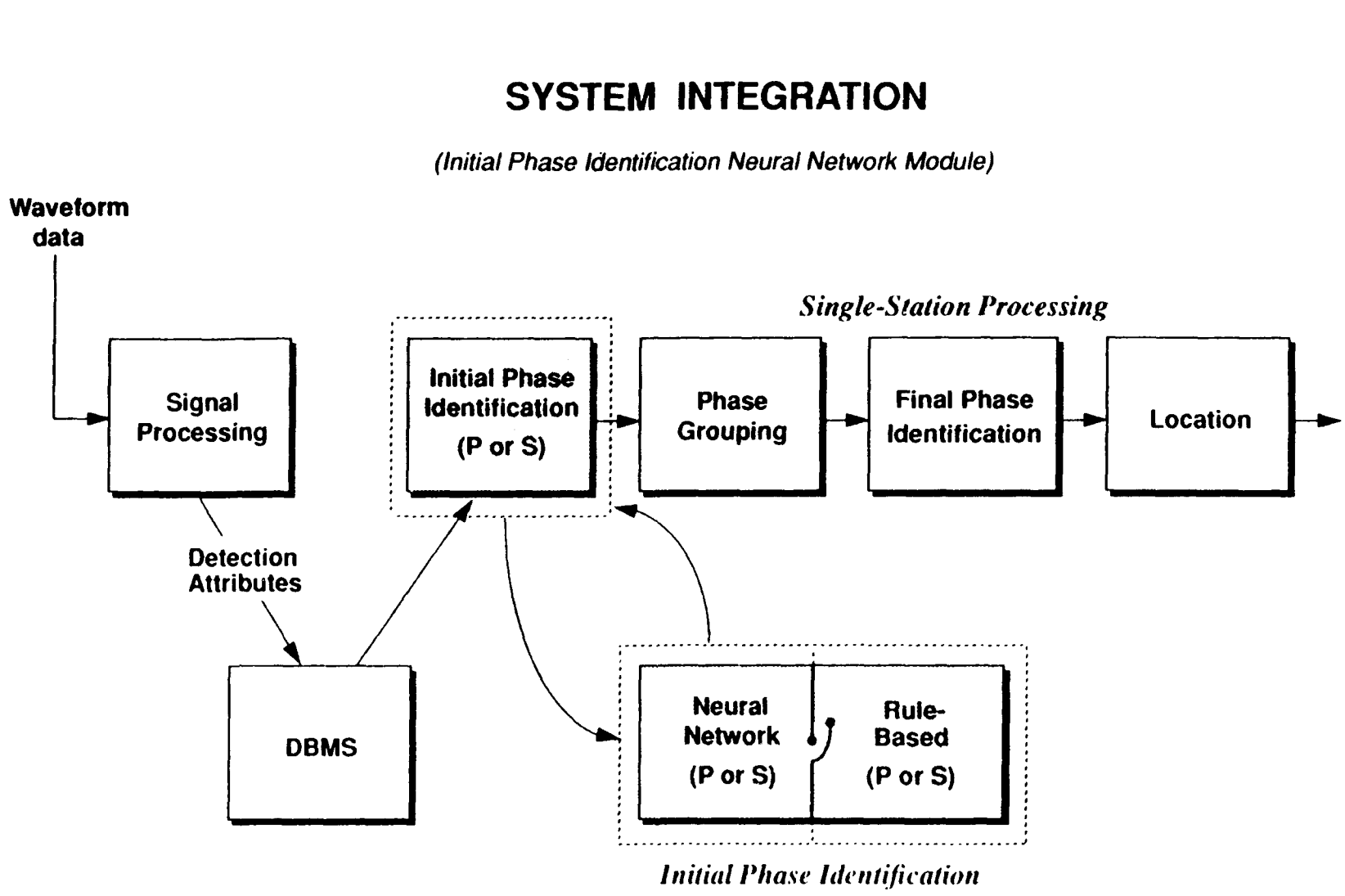

Figure 1. *System Integration (Station Processing). Schematic diagram showing station processing in IMS that includes the neural network module for initial phase (P or S) identification for 3-component stations*

The next step is *phase grouping* which forms groups of phases that appear to be generated by the same event. This grouping is combined with the detection attributes to identify regional phases (*Pn, Pg, Px, Sn, Sx, Lg, or Rg*) or teleseismic phases. Finally, the phase associations are used to estimate single-station locations. The implementation of our neural network module has a provision to choose between the neural network and the rule-based methods for *initial phase identification* to facilitate comparative performance evaluation (see Section 2.4).

2.2 Data for Operational Test and Evaluation

Our data set for comparative performance testing consists of 1916 analyst-verified events recorded by 6 IRIS/IDA stations in the former Soviet Union. The event epicenters and the station locations are shown in Figure 2. These events were formed by combining data from the four high-frequency arrays in Europe (ARCESS, NORESS, FINESA, GERESS), a 3-component station in Ksiaz, Poland (KSP), and 6 IRIS/IDA broad-band 3-component stations in the former Soviet Union [Ala-Archa (AAK), Arti (ARU), Garm (GAR), Kislovodsk, Western Caucasus (KIV), Obninsk (OBN), and Talaya (TLY)]. The analysis procedure and the resulting analyst-reviewed event bulletin are described by *Swanger, et al.* [1992]. The azimuths obtained from 3-component data are not often reliable, and therefore, single-station events are not often accurately located. However, the general concentration of seismicity closer to the stations is apparent in Figure 2. About 92% of the associated phases from these IRIS/IDA stations that were used for training and testing of the neural networks had $snr > 2$, and most were from two of the stations, AAK and GAR. Figures 3–12 show histograms of the data attributes for *P*-type and *S*-type phases from these 6 stations. The number of *P*-type and *S*-type phases that are used from each station are shown in parentheses, and range from only a few to several hundred. For example, there are only 4 associated *S*-type phases at ARU. In addition to noticeable stations-dependence in these data, these histogram distributions show considerable overlap for *P*-type and *S*-type phases. Detailed descriptions of the polarization and context parameters are given by *Patnaik and Sereno* [1991].

IMS - IRIS/IDA NETWORK

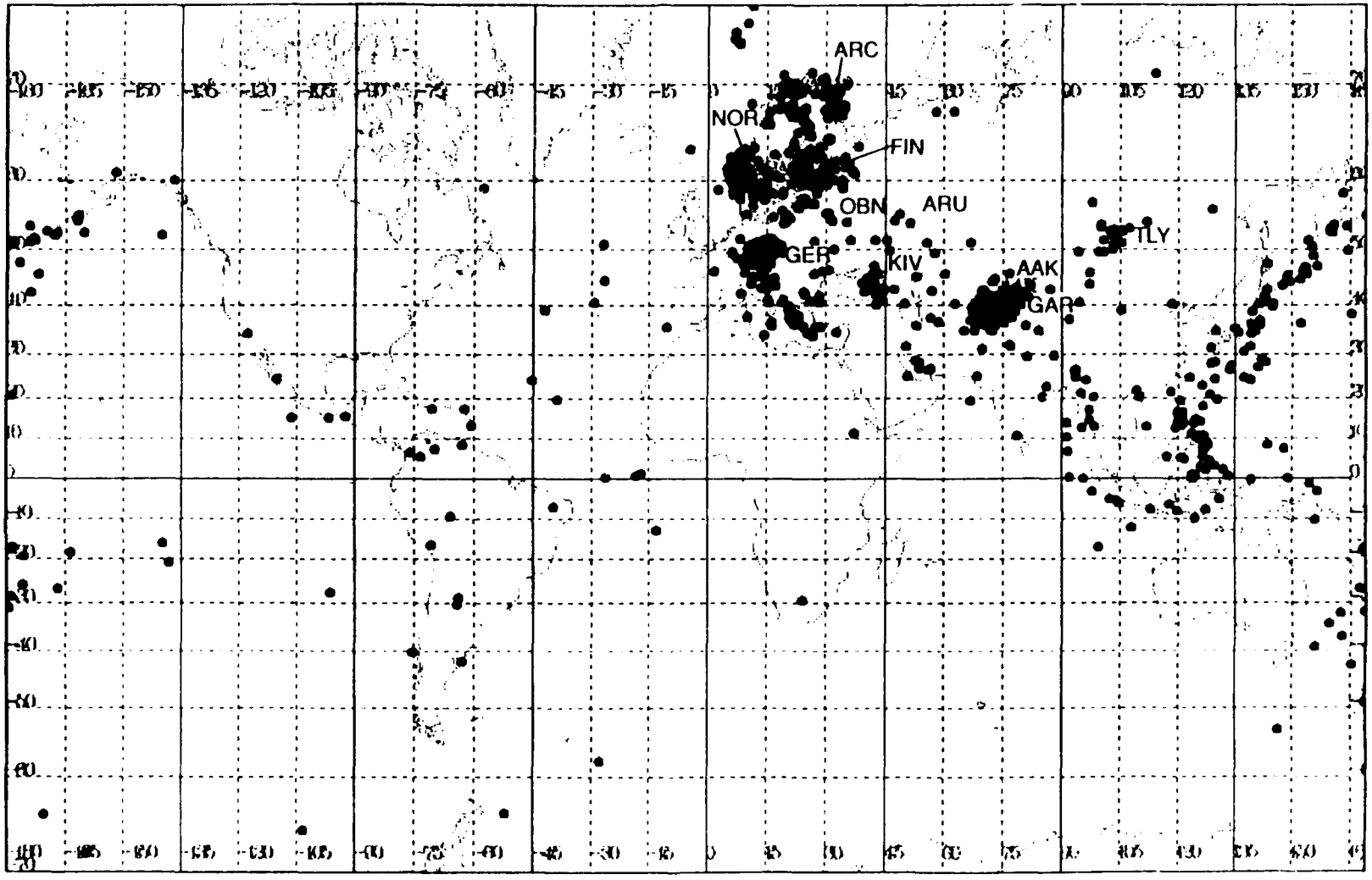

Figure 2. *IMS - IRIS/IDA Network. 1,916 analyst-verified events (solid circles) are shown for the time period between May 21 and Jun 30, 1991. Initial phase identification (P or S) for these events recorded at six IRIS/IDA stations (AAK, ARU, GAR, KIV, OBN, TLY) were carried out by trained Neural Networks*

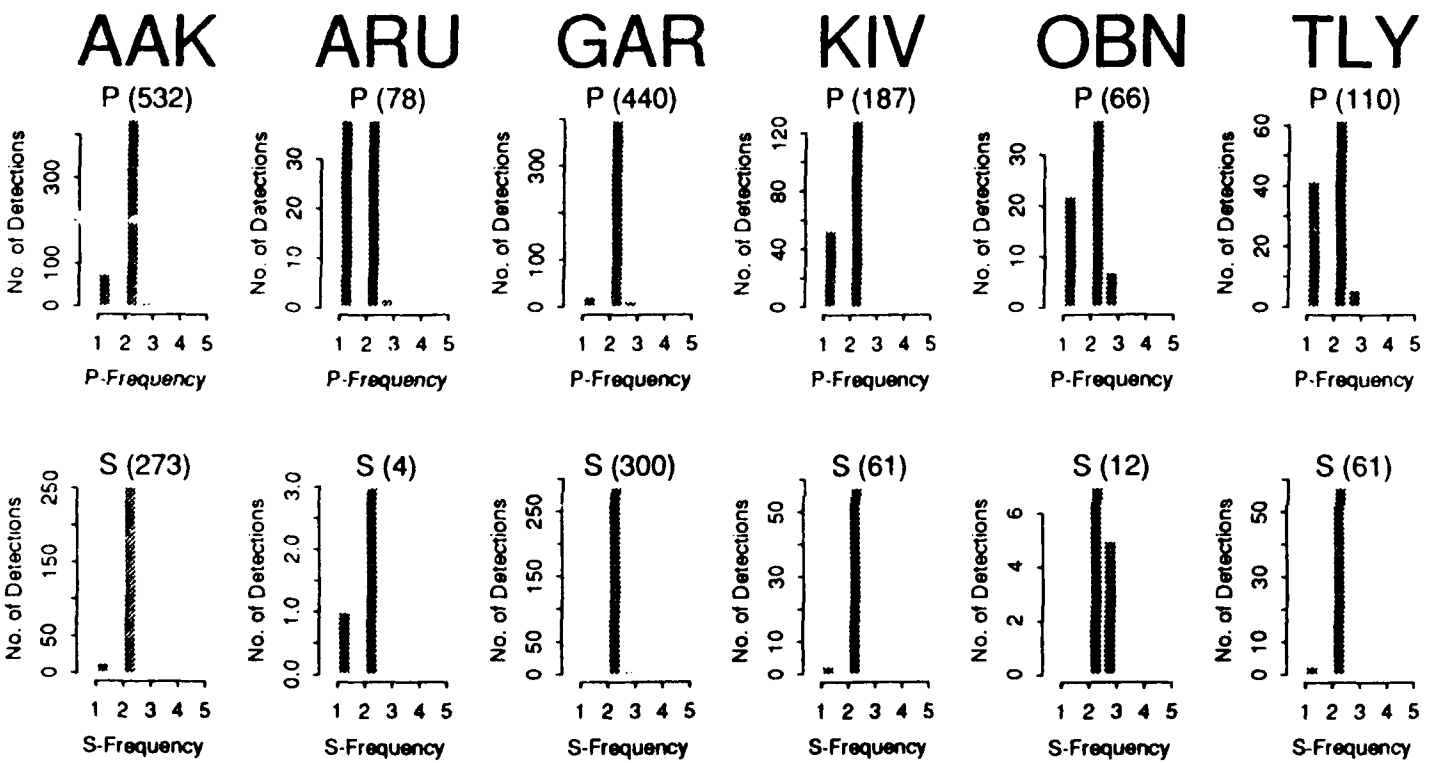

Figure 3. *Histograms of "center frequency of the passbands" are shown for P-type phases (upper) and S-type phases (lower). The numbers in parentheses indicate the number of associated phases. The P and S populations show overlaps at all observing stations.*

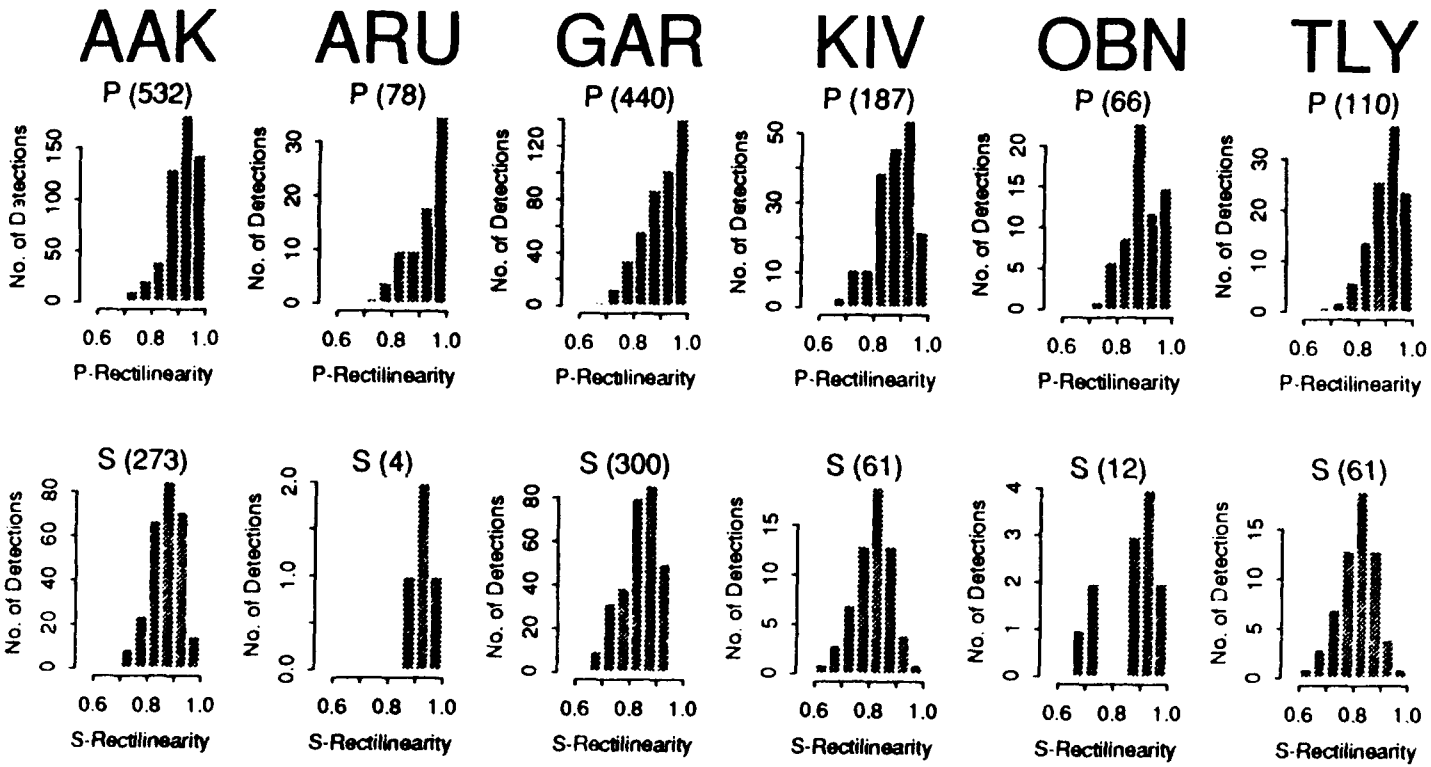

Figure 4. *Histograms of "rectilinearity" are shown for P-type phases (upper) and S-type phases (lower). The numbers in parentheses indicate the number of associated phases. The P and S populations show overlaps at all observing stations.*

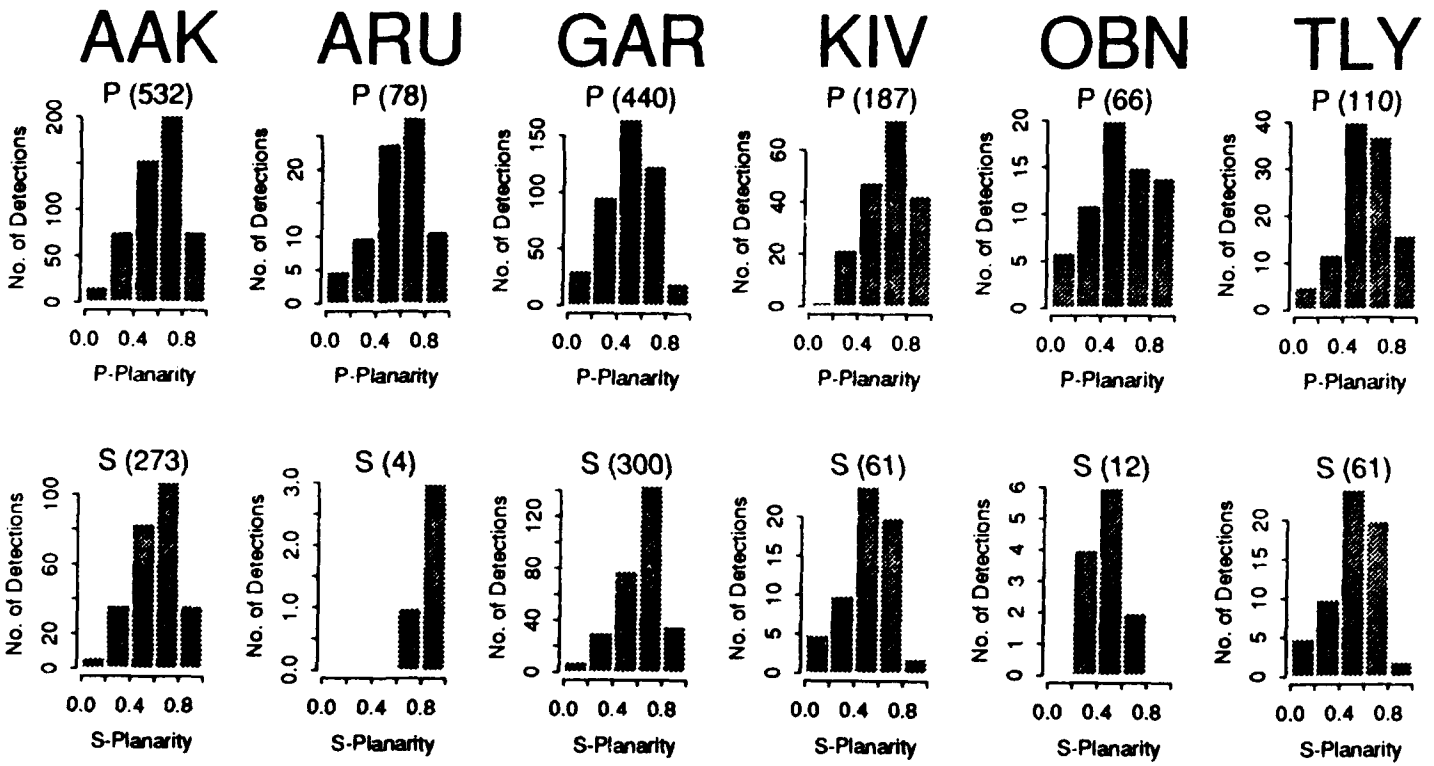

Figure 5. *Histograms of "planarity" are shown for P-type phases (upper) and S-type phases (lower). The numbers in parentheses indicate the number of associated phases. The P and S populations show overlaps at all observing stations.*

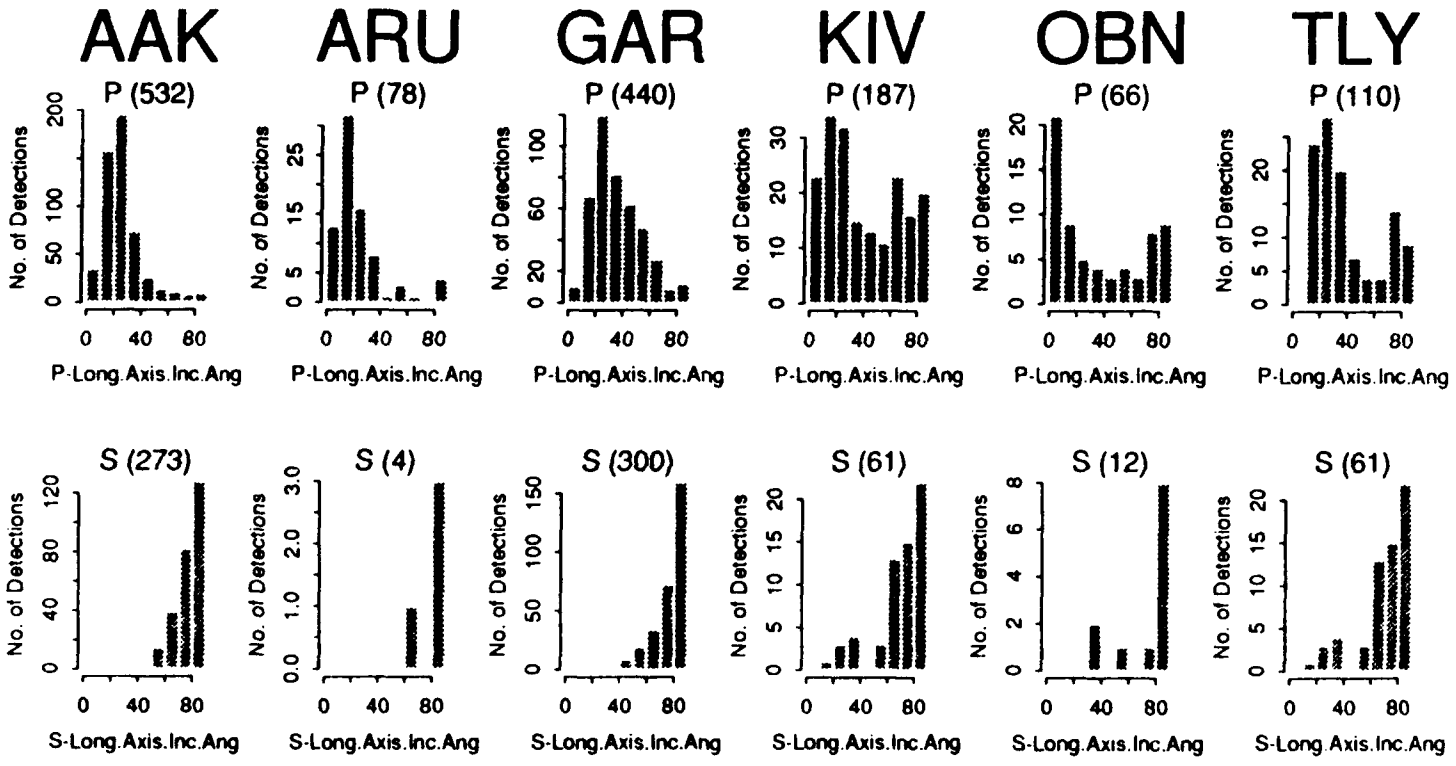

Figure 6. *Histograms of "long-axis incidence angle" are shown for P-type phases (upper) and S-type phases (lower). The numbers in parentheses indicate the number of associated phases. The P and S populations show overlaps at all observing stations.*

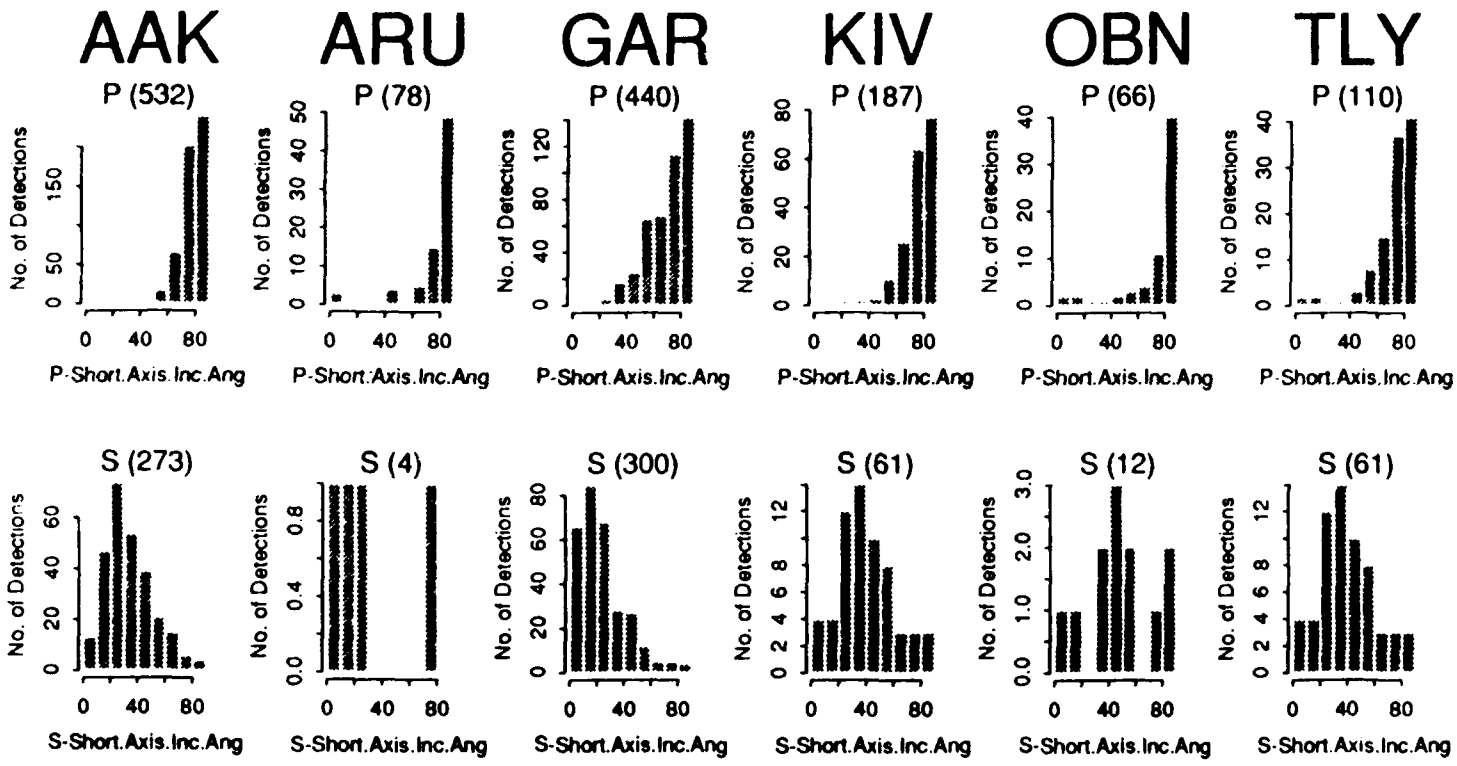

Figure 7. *Histograms of "short-axis incidence angle" are shown for P-type phases (upper) and S-type phases (lower). The numbers in parentheses indicate the number of associated phases. The P and S populations show overlaps at all observing stations.*

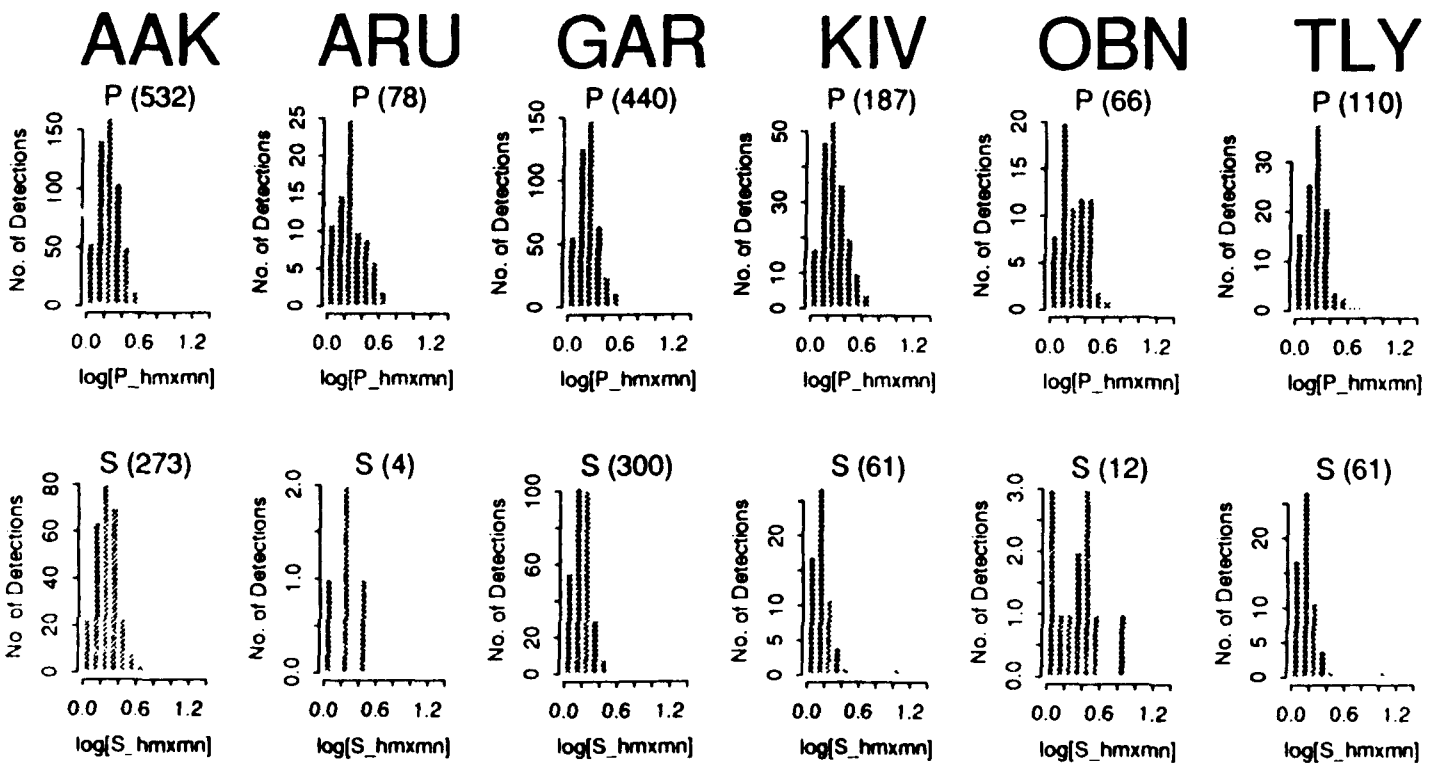

Figure 8. *Histograms of "logarithm of the ratio of maximum to minimum horizontal amplitude" are shown for P-type phases (upper) and S type phases (lower). The numbers in parentheses indicate the number of associated phases. The P and S populations show overlaps at all observing stations.*

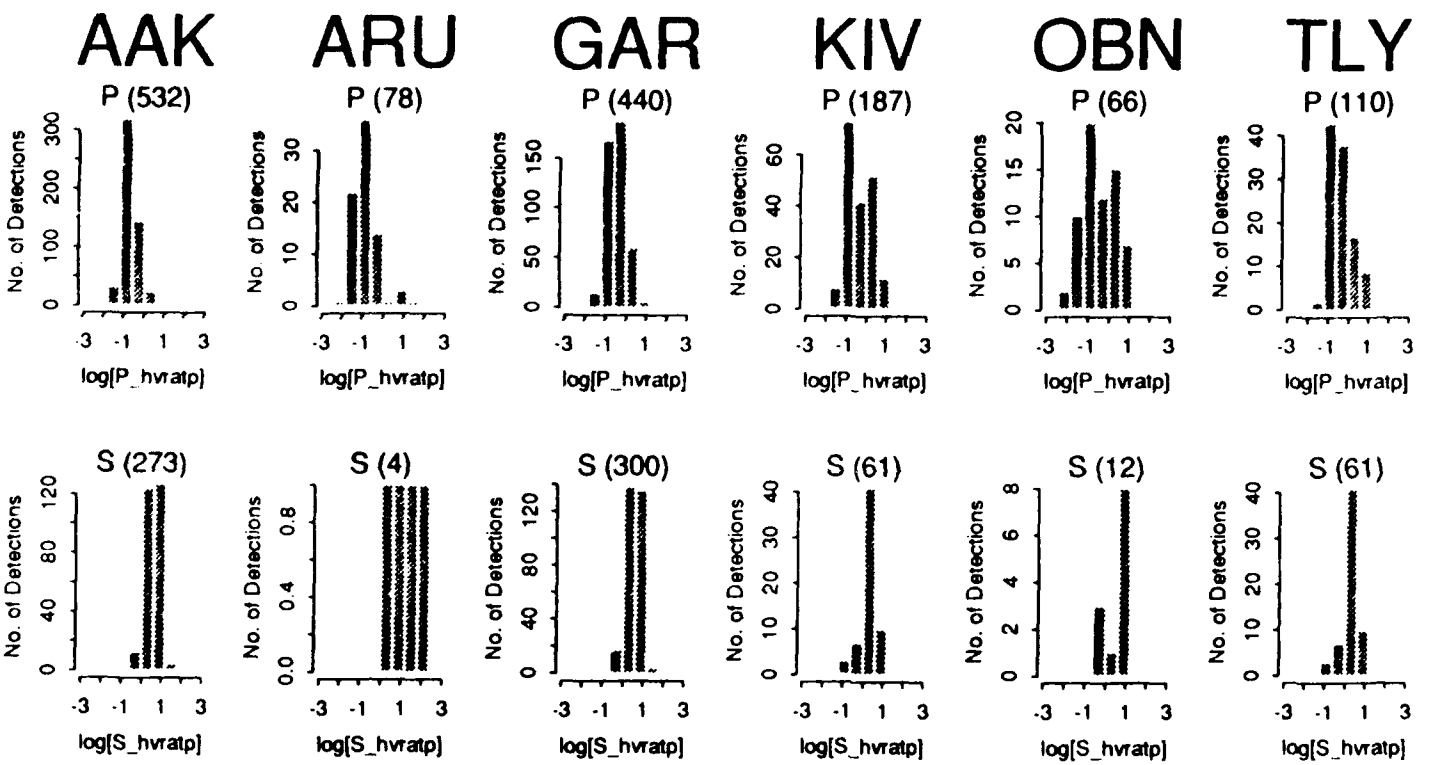

Figure 9. *Histograms of "logarithm of the ratio of horizontal to vertical power at the time of maximum rectilinearity" are shown for P-type phases (upper) and S-type phases (lower). The numbers in parentheses indicate the number of associated phases. The P and S populations show overlaps at all observing stations.*

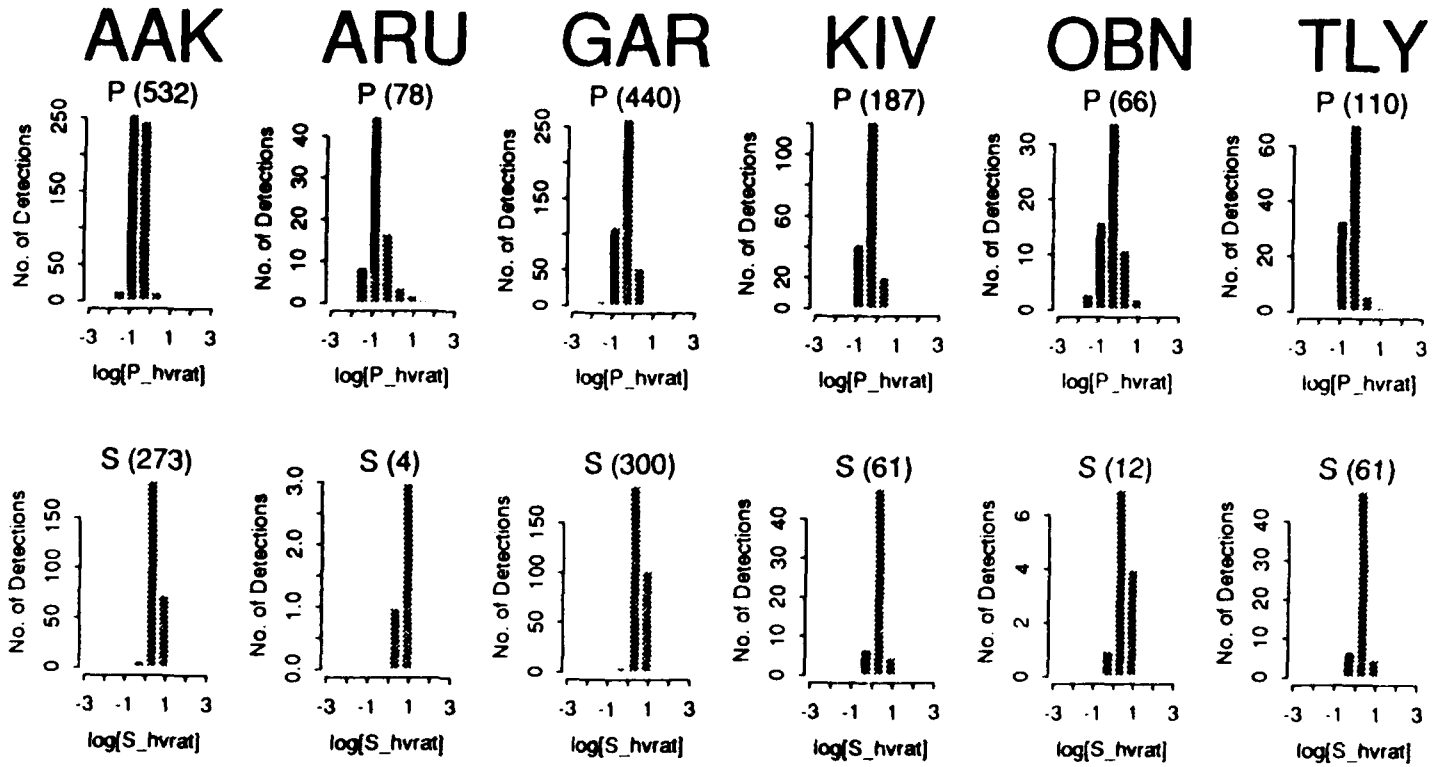

Figure 10. *Histograms of "logarithm of the ratio of horizontal to vertical power" are shown for P-type phases (upper) and S-type phases (lower). The numbers in parentheses indicate the number of associated phases. The P and S populations show overlaps at all observing stations.*

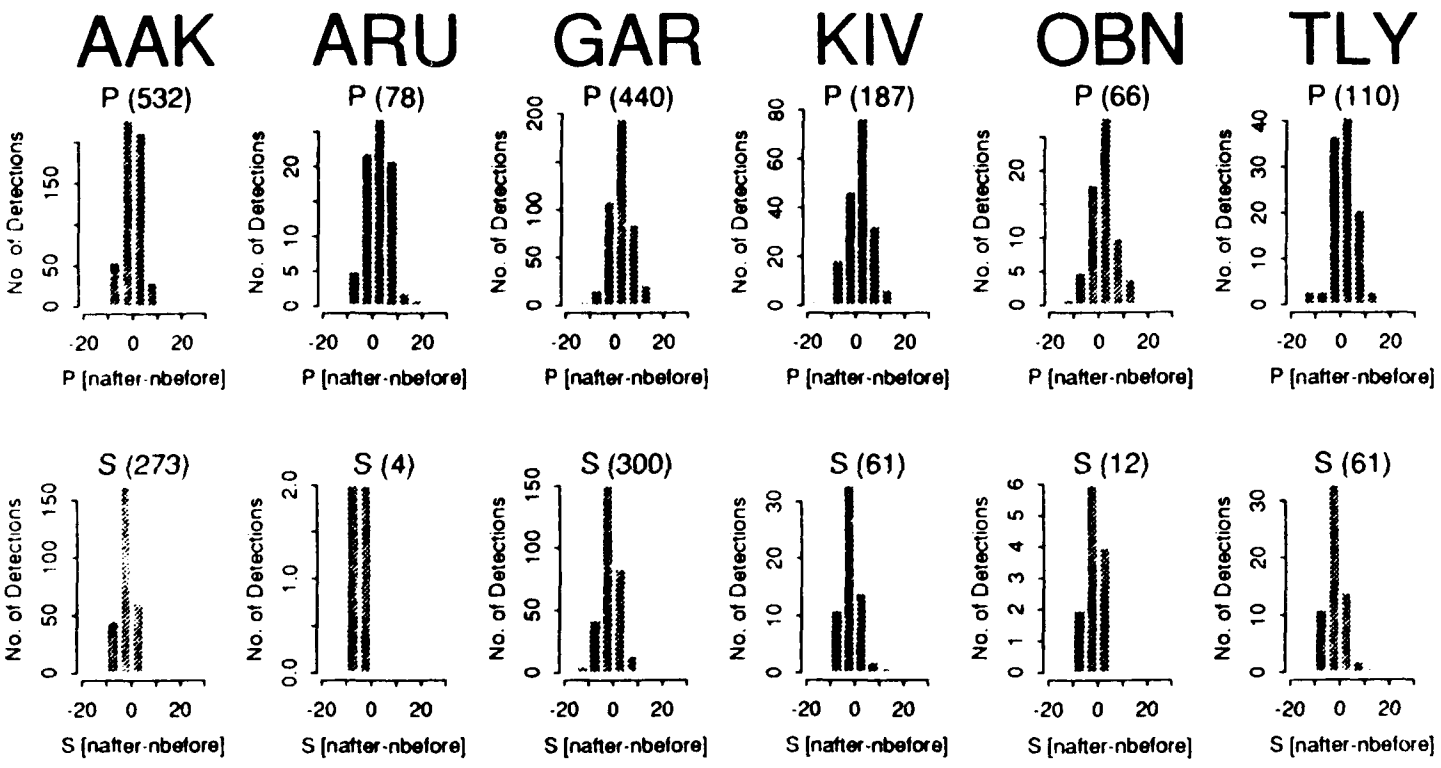

Figure 11. *Histograms of the difference between the number of detections that arrive after and before the detection in question (P-type, upper pannel and S-type, lower pannel), within a fixed time window of 60 seconds. The window length is dependent on seismicity observed at a station. However, for an IRIS/IDA station, a fixed window of 60 seconds was used because of the lack of data.*

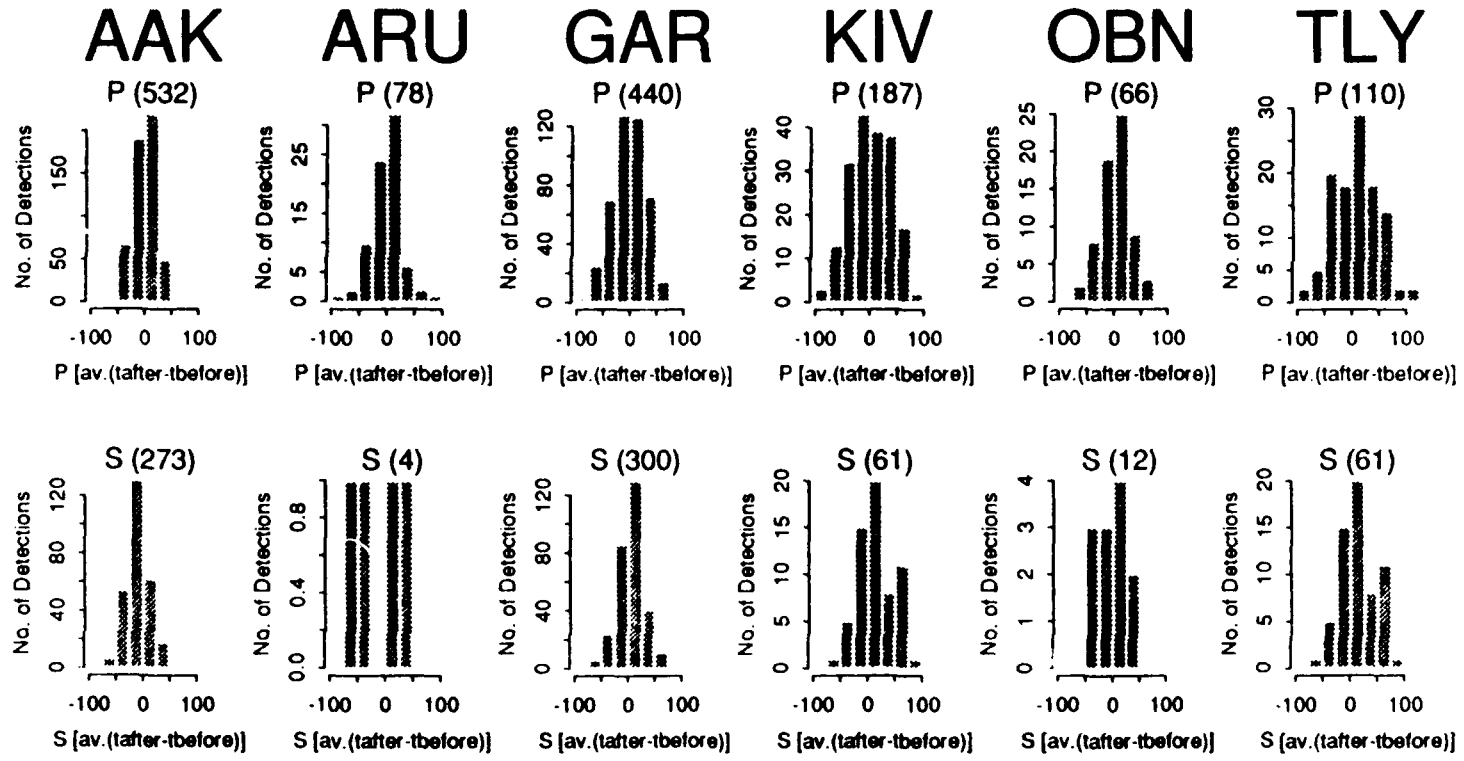

Figure 12. *Histograms of the difference between the average arrival times after and before the detection in question (P-type, upper pannel and S-type, lower pannel), within a fixed time window of 60 seconds. The window length is dependent on seismicity observed at a station. However, for an IRIS/IDA station, a fixed window of 60 seconds was used because of the lack of data.*

2.3 Neural Network Training

The neural networks are trained with the input parameters described in the previous sections under the assumption that the phase labels assigned by an analyst are *ground truth*. The neural network software module includes a provision for station-dependent weights (e.g., separate weights derived from neural networks trained for each station). However, only two of the IRIS/IDA stations had enough analyst-reviewed data for reliable training and testing (AAK and GAR). For the remaining four stations (ARU, KIV, OBN, TLY), we developed average weights by using data combined from all 6 stations.

Figure 13 shows the schematic view of the resulting 3-layer neural network architecture (10-6-2) for the station GAR. The final weight configurations (the two weight matrices) are derived by using the method described by *Patnaik and Sereno* [1991]. The equations shown to the right in Figure 13 determine the activation values at the nodes when an input vector is fed-forward through a trained neural network. As shown in this figure, the higher activation (0.99) of the *P*-output node implies that the input vector for this detection is characteristic of a *P*-type phase.

Table 1 shows the adaptability of the neural network approach for initial phase identification to data from new stations. The matrix is for the 6 IRIS/IDA stations and the combined average case (denoted by IRIS in Table 1). The diagonal elements show the average percentage of correct identification of the phases for training and testing with data from the same station. The off-diagonal percentages are the results of adaptability testing. As it was seen earlier for the array stations [*Patnaik and Sereno*, 1991], the identification accuracy is about 10-15% higher if training and testing use data from the same station. A trained network generally shows about 75–85% correct phase identification accuracy if applied to data from a new site. Thus, the propagation characteristics may be similar for all geological environments tested, to the extent that 75–85% of the detections have similar polarization and contextual characteristics. The rest of the increase by 10-15% upon retraining may be attributed to the site-specific characteristics of the 6 different regions in the former Soviet Union. Apart from this general observation, it is noteworthy that even with the average weights, the actual identification accuracy at any of the 6 IRIS/IDA stations remains close to 90%. Another observation from these results is that even with few *ground truth* data (e.g., at ARU, KIV, OBN, or TLY) a neural network can be trained and adapted to a new site with close to 80% identification accuracy for the new data, which is significant from the viewpoint of rapid deployment of monitoring stations. Enough data can be accumulated for retraining within a few weeks of continuous station operation, and training takes <30 minutes on a Sun Sparc Station.

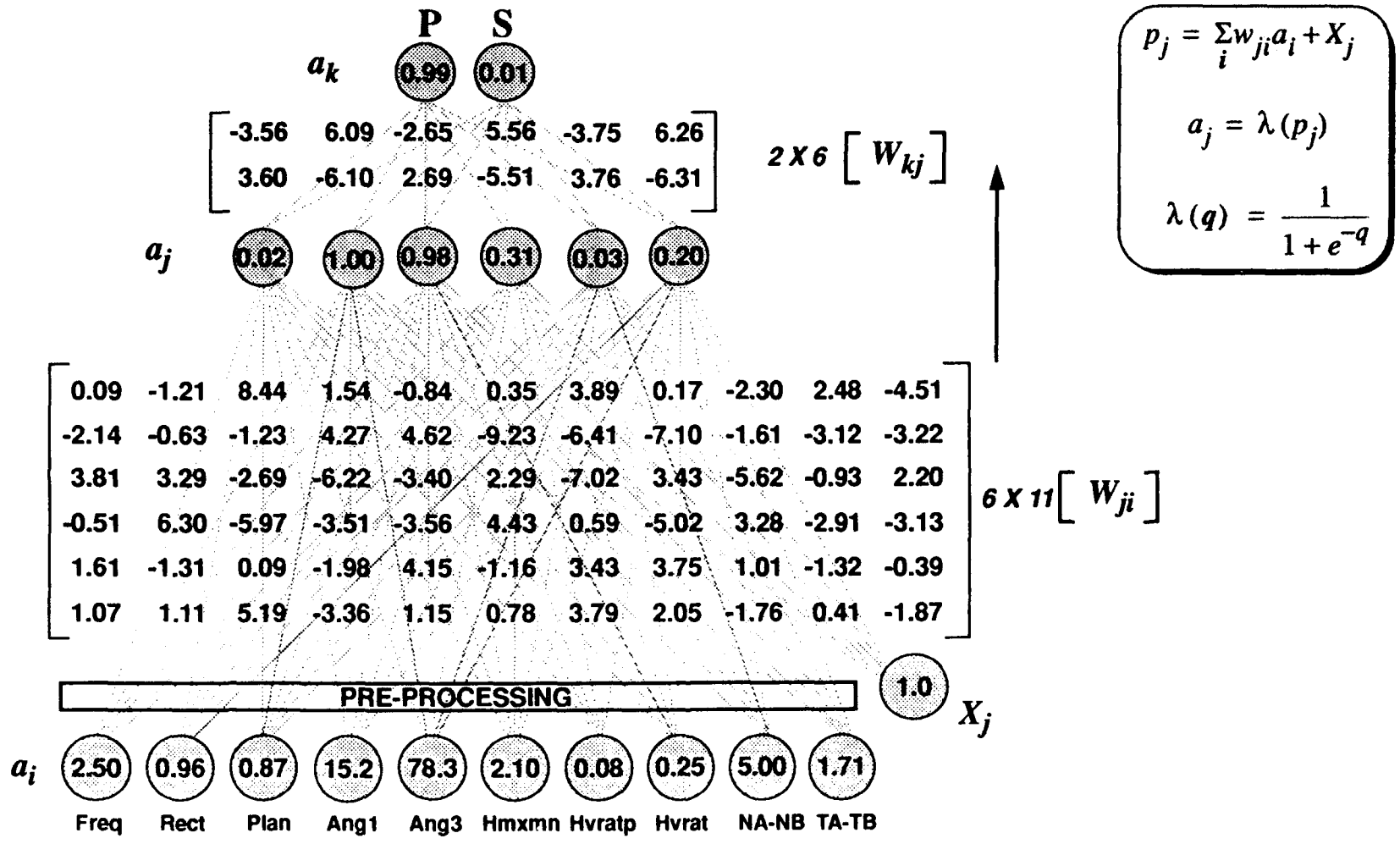

Figure 13. *Schematic diagram of a trained, 3-layer, feed-forward Neural Network (10-6-2). The input nodes are a_i (polarization and context attributes); w_{ji} are the weights from input to middle (hidden) layer; a_j are the middle-layer nodes; w_{kj} are the weights from middle to output layer; and a_k are the output nodes (P or S). This particular example shows the identification of a P-type phase at Garm (GAR).*

Table 1.

ADAPTABILITY TESTING FOR THE IRIS/IDA STATIONS IN THE FORMER SOVIET UNION

(Average Percentages of Correct Identification of Both P-type and S-type Phases)

Test / Train	IRIS (2102)	AAK (805)	ARU (82)	GAR (740)	KIV (248)	OBN (78)	TLY (149)
IRIS	94.3	97.1	92.2	94.2	90.7	88.5	91.8
AAK	88.3	99.5	89 .0	86.5	76.6	78.2	83.6
ARU	84.1	83.0	100.0	79.2	81.5	84.6	71.4
GAR	92.0	94.4	93.9	97.0	78.2	75.6	81.3
KIV	89.4	92.0	86.6	84.5	99.2	83.3	90.6
OBN	84.4	84.1	93.9	79.7	81.0	100.0	74.3
TLY	80.9	80.0	79.3	83.9	82.3	68.0	100 .0

On average, 10-15% increase in correct identification occurs if the network for a station is retrained with data from that station, as opposed to adapting weights from another station. The perfect accuracy (100%) obtained for the stations ARU, OBN, and TLY is the artifact of too few training samples (ground truths). The numbers in parentheses below each station denote the number of analyst-verified training samples (P and S phases) available for that station.

2.4 Results of Operational Testing

For operational test and evaluation, the *IMS* was applied to the 6-week period of continuous data between 21 May 1991 and 30 June 1991. It was done twice; once with the rule-based method for initial phase identification, and once using the trained neural networks. The results of initial phase identification accuracy and the automated event bulletins were compared to the analyst-produced bulletin.

In general, the neural network performed better than the rule-based method in *IMS* by about 3–6%. For example, Table 2 shows the *confusion matrices* for the initial phase identifications for AAK, GAR, and all 6 IRIS/IDA station data combined. The tables on the left show the results of the rule-based expert system (ES), and the tables on the right show the results for the neural network (NN). These results are also displayed graphically in Figure 14. The bar-graphs represent the results in percentages of correct identification of phases. The identification accuracy using the average weights (combined data from all stations) is not as high as it is for AAK and GAR, but it is higher than it is in the current rule-based system. The average weights will be replaced with station-specific weights as more analyst-reviewed data become available (these data are currently being processed and analyzed at CSS). The final identification accuracy is >95% for each individually-trained station.

The neural networks averaged 3.9% better than the ESAL rules for initial phase identification for all 6 IRIS/IDA stations. However, it performed 6.3% better in identifying *P* phases which are more important for teleseisms (*P* and *S* are about equally important for regionals, but it is more important to identify *P* phases correctly for events recorded at multiple stations). Table 3 shows the identification accuracy for *P* phases, *S* phases and the average of both, for each of the 6 IRIS/IDA stations and for all stations combined. For the stations ARU, KIV, OBN, and TLY, the average weights were used for initial phase identification. These results are slightly different from those shown in Table 1 because the data in the time interval used for our operational test was slightly different.

Table 4 shows the comparison of the event bulletins produced when the neural network was used for initial phase identification (NN) and when the current *IMS* rule-based expert system was used (ES). Close to 75% of the events in the ES and NN bulletins are identical. Here we focus on the comparison of the other 25% to the analyst-reviewed bulletin (AN). The NN bulletin was closer than the ES bulletin to the AN bulletin. The most important difference is that only 2.1% of the analyst events were missed by the NN, whereas 5.3% were missed by the ES. The difference is 61 events during the 6-week interval, or about 10 events/week. Also, more of the events formed by the automated processing were accepted by the analyst when the neural network was used for initial phase identification. The last row in Table 4 lists events that were in the automated bulletin, but were not in the analyst bulletin. However, since the analysis was restricted primarily to events recorded by at least two stations [*Swanger et al.*, 1992], it is not possible to determine how many of these are true events as opposed to false-alarms.

Table 2.

CONFUSION MATRICES

(Initial Phase Identification Neural Network)

AAK

Analyst	ES P	ES S	Total
P	515	17	532
S	10	264	274
Total	525	281	806

Analyst	NN P	NN S	Total
P	527	5	532
S	3	271	274
Total	530	276	806

GAR

Analyst	ES P	ES S	Total
P	379	61	440
S	4	297	301
Total	383	358	741

Analyst	NN P	NN S	Total
P	429	11	440
S	11	290	301
Total	440	301	741

6 IRIS/IDA Stations Combined

Analyst	ES P	ES S	Total
P	1,281	133	1,414
S	24	668	692
Total	1,305	801	2,106

Analyst	NN P	NN S	Total
P	1,370	44	1,414
S	31	661	692
Total	1,401	705	2,106

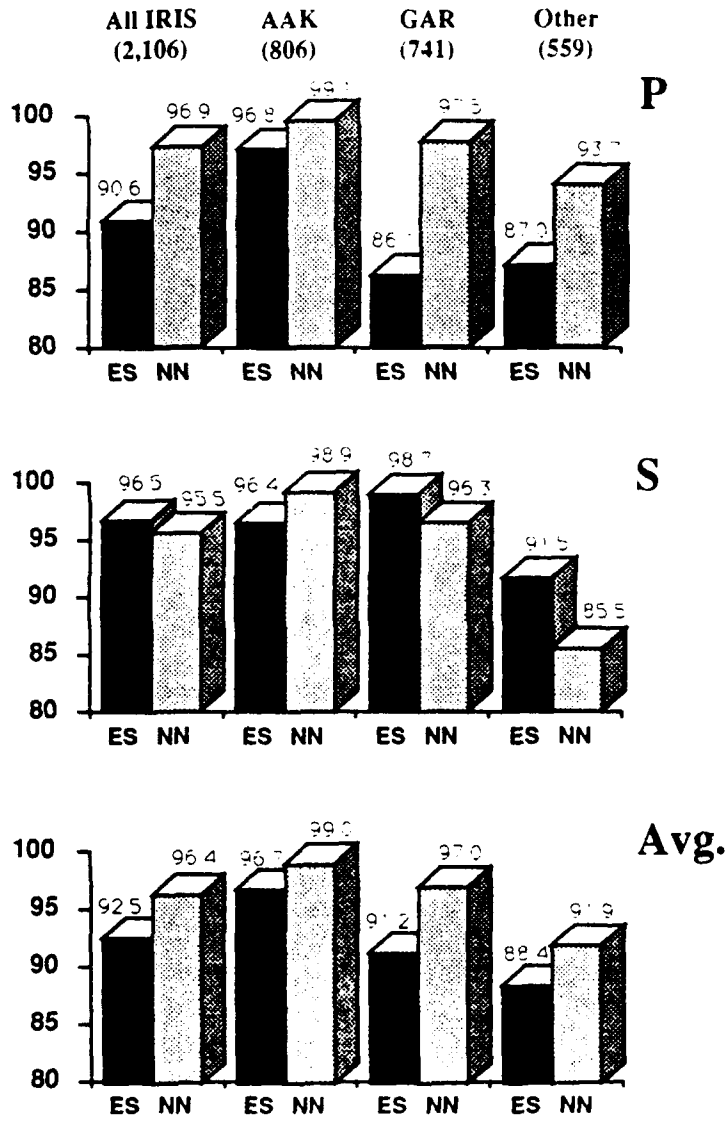

Figure 14. *Results of operational testing of the Neural Networks for initial phase identification for 3-component stations in IMS. The vertical axis represents percentages of correct identification. On the horizontal axis, ES denotes rule-based method and NN denotes Neural Network method.*

Table 3.

NEURAL NETWORK VS. RULE-BASED INITIAL PHASE IDENTIFICATION

	Station	AAK	ARU	GAR	KIV	OBN	TLY	All IRIS (combined)
	Total Number of P & S Phases (Ground Truths):							
		806	82	741	249	78	150	2,106
Neural Network	**P%**	99.0	93.6	97.5	93.6	92.4	94.5	96.9
	S%	98.9	100	96.3	88.5	83.3	80	95.5
	Average%	**99.0**	**93.9**	**97.0**	**92.4**	**91.0**	**90.7**	**96.4**
Rule-Based	**P%**	96.8	91	86.1	86.2	80.3	91.8	90.6
	S%	96.4	100	98.7	91.8	91.7	90	96.5
	Average%	**96.7**	**91.5**	**91.2**	**87.6**	**82.1**	**91.3**	**92.5**

Table 4.

BULLETIN COMPARISON

(Initial Phase Identification Neural Network)

NEURAL NETWORK (NN) AND RULE-BASED (ES) VS. ANALYST

Analyst Action	NN	ES
Accepted	838	806
Modified	1,037	1,008
Added[+]	41	102
Rejected *or* Ignored	5,238	5,246

[+] *Only 15 of the analyst-verified events were missed by both the NN and the ES. There were 87 events in NN that were not in ES and 32 of these were recorded at ≥ 2 stations. There were 26 events in ES that were not in NN, and 20 of these were recorded by ≥ 2 stations.*

In summary, the increase in the phase identification accuracy provided by the neural network technique also improved the final automated event bulletin (particularly by reducing the number of events missed by the automated processing). The analyst accepted more of the events formed by the automated system when the neural network was used for initial phase identification, and fewer events were missed by the automated processing. Larger gains are expected once enough data are available at all IRIS/IDA stations to derive a full set of station-specific weights. Also, the analysis procedures only included events recorded at ≥2 stations with at least 3 defining-phases, so the test database is biased towards high *snr* (about 92% of the associated phases in the test database had $snr > 2$). The improvement offered by the neural networks is greater for low *snr*, so larger gains are expected for routine analysis of data from all stations.

3. REGIONAL PHASE ID NEURAL NETWORK MODULE

MIT/Lincoln Laboratory developed and trained a neural network for automated identification of regional seismic phases recorded by high-frequency arrays under DARPA's *ANNT* Program [*Lacoss, et al.*, 1990; *Lacoss, et al.*, 1992]. The purpose was to improve the automated performance of the *IMS* by providing more accurate regional phase identifications (e.g., *Pn, Pg, Px, Sn, Sx, Lg, Rg*). We developed a joint plan with MIT/Lincoln Laboratory to implement, test and evaluate the performance of their neural network module in *IMS* under operational conditions. In this section we describe the implementation, and give results from our operational testing.

3.1 Technique

Figure 15 is a schematic diagram showing station-processing in *IMS* with the inclusion of MIT/Lincoln Laboratory's neural network for final phase identification. Most of the steps involved in station processing were described in Section 2. The main point is that this neural network module is used in parallel with the current *IMS* rule-based method to improve the accuracy of the phase identification. That is, the detection attributes and the phase identification determined by the rule-based system are input to the neural network. The output of the neural network is a refined phase identification (with an associated measure of confidence). This refined phase identification is used to estimate a more accurate single-array event location.

SYSTEM INTEGRATION

(MIT/Lincoln Laboratory Regional Phase Identification Neural Network Module)

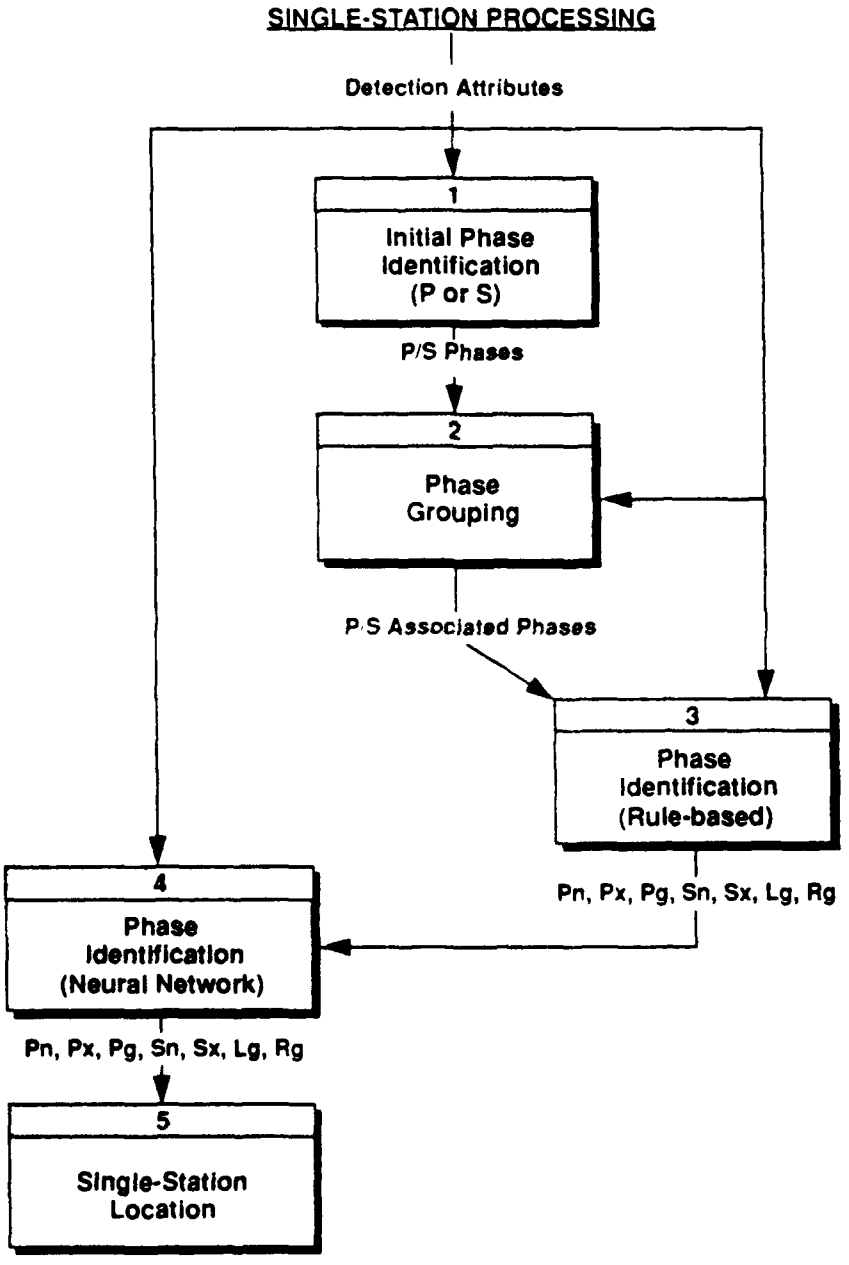

Figure 15. *This is a schematic diagram for single-station processing in IMS that includes the Neural Network approach for regional phase identification (step 4) developed by MIT Lincoln Laboratory.*

3.2 Data for Operational Test and Evaluation

Data recorded by the four European high-frequency regional arrays (ARCESS, NORESS, FINESA, and GERESS) during April, 1991, were used for operational test and evaluation. Table 5 lists the number of detections in the test data set for each array. The first row lists the total number of detections, and the second row lists the number of these that are associated with a regional event. Unfortunately, not all of these have valid polarization or amplitude data in the *IMS* database at the Center for Seismic Studies (CSS). The third row lists the subset of the associated detections that had all data required for input to the neural network. Only about 9% of the total number of detections recorded at the four arrays during April, 1991, could be used for the operational test and evaluation of this module. This is because of the missing data attributes, the nature of the problem being addressed, and the rigid structure of the static neural networks that require fixed number of input parameters where missing data attributes are not allowed. The last row in Table 5 lists the number of these detections where the rule-based phase identification was different than the neural network phase identification. This includes about 8.8% of the detections with valid data.

Table 5.

TEST DATA SET

(Regional Phase Identification Neural Network)

April 1 - 30, 1991

	All Sta.	ARCESS	NORESS	FINESA	GERESS
Total	37,075	17,038	6,735	7,831	5,471
Station assoc. reg. phase	5,306	2,148	926	1,349	883
Valid data (apma, sbsnr)	3,125	1,128	436	954	607
NN (phase) ≠ ES (phase)	274	144	31	60	39

NN Neural Network

ES Rule-based Expert System

Neural Network changes the phase identification of about 8.8% of all detections with valid data.

3.3 Results of Operational Testing

We tested MIT/Lincoln Laboratory's neural network for regional phase identification under simulated operational conditions in an off-line version of *IMS*. This was done by running *ESAL* (where the neural network module actually resides) twice; once without the neural network for station processing (this is equivalent to the normal operation), and once with the neural network. The results of each run were compared to the analyst-reviewed solutions to estimate identification accuracy for each regional phase, and to compare the automated event bulletins.

The overall phase identification accuracy achieved by the neural network is compared to the results of the rule-based system in Table 6. The top half of the table lists the results after *station processing* (*IPHASE*), and the bottom half lists the results after *network processing* (*PHASE*). For this test, we only used detections with valid data attributes and whose *phase grouping* was the same in the analyst bulletin as it was in the pre-analyst (automated) bulletin. This gave about 2500 detections for the one-month test period. The average phase identification accuracy for all stations after *station processing* is 88.7% for the neural network which is about 3.3% higher than the current rule-based system. The most improvement is for ARCESS where the identification accuracy is 6.0% higher for the neural network than it is for the rule-based system. However, the average gain achieved by the neural network drops to about 1.0% after *network processing*. That is, some of the phases that are correctly labeled by the neural network during *station processing* are incorrectly changed during *network processing*. This also happens to a lesser extent for the rule-based system. For example, the identification accuracies for FINESA and GERESS are reduced by *network processing*. However, the opposite is true for ARCESS and NORESS (the network processing rules were based primarily on data from these two arrays). It is likely that greater overall improvement could be achieved by using the neural network confidence estimates in *network processing*.

The phase identification *confusion matrices*, after *station processing*, for the current *IMS* rule-based system and MIT/Lincoln Laboratory's neural network are shown in Tables 7*a* and 7*b*, respectively. The numbers are expressed as a fraction of the total number of phases (shown in the last column). The analyst's phase identifications (*ground truth*) are shown on the left, and the labels determined by automated processing are shown at the top. The diagonal elements indicate the fraction of the total number of phases that were correctly identified by the automated interpretation. The off-diagonal elements represent the fraction of phases that were incorrectly identified. These tables combine data from all stations. Most of the improvement offered by the neural network is in distinguishing between *Sn* and *Sx*, and between *Pg* and *Px*. *Px* and *Sx* are regional *P* and *S* phases that are associated with an event on the basis of slowness and azimuth, but are not associated with a specific travel time branch (e.g., coda detections). Tables 8*a* and 8*b* show the *confusion matrices* after *network processing* for the two methods of phase identification (rule-based and neural network) in *station processing*. The *Neural Network PHASE* in Table 8*b* is actually the final phase identification after the rule-based *network*

Table 6.

OVERALL REGIONAL PHASE IDENTIFICATION ACCURACY

	All Sta.	ARCESS	NORESS	FINESA	GERESS
Rule-based IPHASE	85.4	81.2	86.1	88.6	86.3
Neural Net IPHASE	88.7 (+3.3%)	87.2 (+6.0%)	87.8 (+1.7%)	90.5 (+1.9%)	88.8 (+2.0%)
Rule-based PHASE	85.1	84.2	88.7	85.7	83.8
Neural Net PHASE	86.1 (+1.0%)	85.5 (+1.3%)	89.4 (+0.4%)	86.9 (+1.2%)	84.0 (+0.2%)

Table 7a.

CONFUSION MATRIX FOR RULE-BASED PHASE IDENTIFICATION (*IPHASE*) DETERMINED DURING *STATION PROCESSING*

Average Accuracy = 85.4%

Analyst *PHASE* (Ground Truth)	**Rule-based *IPHASE***							**Number of Data**
	Pn	**Pg**	**Px**	**Sn**	**Lg**	**Rg**	**Sx**	
Pn	**.97**	.03	-	-	-	-	-	702
Pg	.06	**.89**	.04	-	-	-	-	471
Px	.13	.26	**.62**	-	-	-	-	86
Sn	-	.02	-	**.34**	.33	-	.31	178
Lg	-	-	-	.01	**.91**	.02	.06	941
Rg	-	-	-	-	.13	**.77**	.10	52
Sx	-	-	.01	.04	.45	.04	**.45**	89
Number of Data	723	468	72	74	962	66	154	**2,519**

Table 7b.

CONFUSION MATRIX FOR NEURAL NETWORK PHASE IDENTIFICATION (*IPHASE*) DETERMINED DURING *STATION PROCESSING*

Average Accuracy = 88.7%

Analyst *PHASE* (Ground Truth)	**Neural Network *IPHASE***							**Number of Data**
	Pn	**Pg**	**Px**	**Sn**	**Lg**	**Rg**	**Sx**	
Pn	**.97**	.03	-	-	-	-	-	702
Pg	.06	**.89**	.05	-	-	-	-	471
Px	.13	.17	**.70**	-	-	-	-	86
Sn	-	.02	-	**.69**	.29	-	-	178
Lg	-	-	-	.03	**.94**	.01	.02	941
Rg	-	-	-	-	.29	**.69**	.02	52
Sx	-	-	.01	.11	.49	.08	**.30**	89
Number of Data	723	457	83	157	1,000	51	48	**2,519**

Table 8a.

CONFUSION MATRIX FOR FINAL RULE-BASED PHASE IDENTIFICATION (*PHASE*) DETERMINED DURING *NETWORK PROCESSING*

Average Accuracy = 85.1%

Analyst *PHASE* (Ground Truth)	**Rule-based *PHASE***							**Number of Data**
	Pn	**Pg**	**Px**	**Sn**	**Lg**	**Rg**	**Sx**	
Pn	**.94**	.04	.02	-	-	-	-	540
Pg	.01	**.95**	.03	-	-	-	-	436
Px	.04	.48	**.48**	-	-	-	-	69
Sn	-	.01	.01	**.67**	.24	-	.07	169
Lg	-	-	-	.05	**.85**	.03	.07	784
Rg	-	-	-	-	.12	**.88**	-	41
Sx	-	-	.01	.14	.32	.11	**.42**	81
Number of Data	517	472	60	163	736	69	103	**2,120**

Table 8b.

CONFUSION MATRIX FOR FINAL RULE-BASED PHASE IDENTIFICATION (*PHASE*) DETERMINED DURING *NETWORK PROCESSING*

[when the Neural Network was used for phase identification during *Station Processing* (i.e., for *IPHASE* of Table 7b)]

Average Accuracy = 86.1%

Analyst *PHASE* (Ground Truth)	**Neural Network *PHASE***							**Number of Data**
	Pn	**Pg**	**Px**	**Sn**	**Lg**	**Rg**	**Sx**	
Pn	**.94**	.04	.02	-	-	-	-	541
Pg	.01	**.95**	.03	-	-	-	-	436
Px	.04	.49	**.46**	-	-	-	-	69
Sn	-	.01	.01	**.73**	.21	-	.03	168
Lg	-	-	-	.05	**.87**	.01	.06	787
Rg	-	-	-	-	.32	**.66**	.02	44
Sx	-	-	.01	.12	.36	.10	**.41**	81
Number of Data	518	473	59	171	767	48	90	**2,126**

processing, where the neural network was used in *station processing*. The drop in identification accuracy after *network processing* is primarily caused by incorrectly renaming *Lg* to *Sx*. Depending on the number of defining phases, this may or may not significantly affect the network location.

The automated event bulletins produced using the two methods for regional phase identification are compared with the analyst event bulletin in Table 9. The final bulletin produced using the neural network (NN) is not much different from the bulletin produced by the conventional rule-based system (ES). For example, 95% of the 2142 events formed using the neural network are identical to events formed with the rule-based system. A comparison between the automated and analyst event bulletins (AN) for the remaining 5% is shown in the bottom portion of Table 9. Only 7 events in the AN bulletin were in the NN bulletin, and not in the ES bulletin. Similarly, 5 events in the AN bulletin were in the ES bulletin, but not in the NN bulletin. There are 87 events that are in all three bulletins, but the ES location is not the same as the NN location. The NN location is closer to the AN location than the ES location for only slightly more than half of these. For example, the average difference in distance between the AN location and the NN location for these events (*ddist*) is 103.9 km, and it is 135.4 km for the ES location. Therefore, the neural network did only slightly better than the rule-based system on the 5% of the events that were different. However, we expect more improvement if the neural network confidence measures were used in *network processing*.

Table 9.

BULLETIN COMPARISONS

(Regional Phase Identification Neural Network)

2,130 Events in ANALYST BULLETIN (AN)
2,142 Events in NEURAL NET BULLETIN (NN)
2,145 Events in RULE-BASED BULLETIN (ES)

2,031 Events where NN = ES (95%)

126 Events where NN ≠ ES (5%)

- **12 Events in NN BULLETIN, but not in ES BULLETIN**
  - 7 are in AN BULLETIN
  - 5 are not in AN BULLETIN

- **15 Events in ES BULLETIN, but not in NN BULLETIN**
  - 5 are in AN BULLETIN
  - 10 are not in AN BULLETIN

- **99 Events are in ES and NN, but ES ≠ NN**
  - 12 are not in AN BULLETIN
  - 87 are in AN BULLETIN

47% have ES closer to AN than NN
53% have NN closer to AN than ES

Rule-based vs. Analyst

N	=	87	
MEAN ddist	=	135.4	km
MEDIAN ddist	=	43.8	km
MEAN dtime	=	16.5	s
MEDIAN dtime	=	5.1	s

Neural Net vs. Analyst

N	=	87	
MEAN ddist	=	103.9	km
MEDIAN ddist	=	28.2	km
MEAN dtime	=	11.3	s
MEDIAN dtime	=	2.9	s

4. REGIONAL SEISMIC EVENT IDENTIFICATION

We conducted a preliminary study on the application of neural networks to identify regional events on the basis of their broad-band envelope shape. *Patnaik* [1989] applied a similar approach to identify Love and Rayleigh surface wave trains from single-station recordings of oceanic earthquakes. A neural network classifier based on the envelope shape of these waves consistently performed perfect identification on different test data. A number of recent studies [e.g., *Dowla, et al.*, 1990; *Dysart and Pulli*, 1990; and *Lacoss, et al.*, 1990; *Patnaik, et al.*, 1990] report the use of neural network classifiers for seismic event recognition with learning from previously known patterns.

4.1 The Discriminant

It is observed that the coda decay rate is generally lower for earthquakes than it is for explosions. For example, *Su, et al.*, [1991] observe that the coda decay rate is significantly higher for quarry blasts than for earthquakes at low frequencies (1.5 to 3 Hz) for lapse time up to about 30s. Although these observations were made from carefully studied events at short epicentral distances, visual inspection of a large number of seismograms recorded at GERESS from near-regional to far-regional distances from known mining regions and seismically active regions reveal a similar pattern of coda decay rate. For example, Figure 16 shows an example of earthquake and explosion recordings from GERESS. The epicentral distances are similar (490 km for the earthquake, and 350 km for the presumed explosion), and the shape of the *P*-coda is much different. This simple observation motivated us to examine if we could utilize this difference in the shape of the coda to discriminate between earthquakes and explosions.

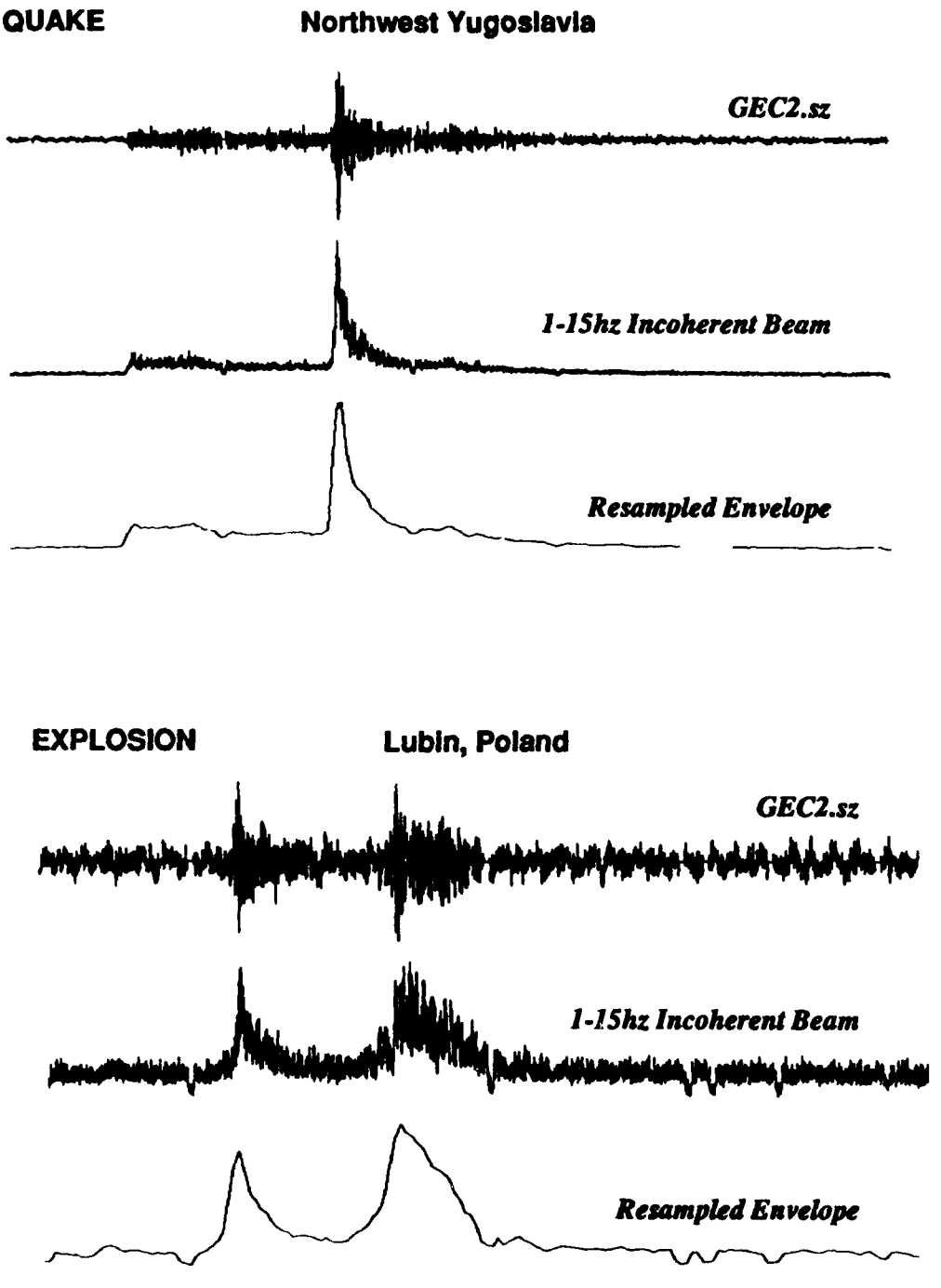

Figure 16. *The three traces in the upper panel are, from top to bottom, a short-period vertical channel (GEC2) seismogram, a 1-15hz incoherent beam (formed from all 25 vertical channels), and a resampled and smoothed envelope of a presumed earthquake in northwest Yugoslavia recorded at GERESS. Similarly, the bottom panel displays respective traces for a presumed explosion in Lubin, Poland.*

4.2 Data

We developed and conducted preliminary tests of our neural network approach using data from 61 regional events recorded at GERESS. Figure 17 shows the locations of these events and the location of the GERESS array. The solid circles represent 35 presumed explosions at the Polish mining districts (e.g., Lubin and Dubna Skala). Our *ground truth* is based purely on the assumption that events occurring near these mining regions are probable explosions. However, it is possible that some of these may actually be mining-induced earthquakes [e.g., *Bennett et al.*, 1992; and Dr. H-P. Harjes, personal communication]. Similarly the assumption of *ground truth* for 26 earthquakes (solid squares) is based on the general seismicity to the south of GERESS. Although there is uncertainty in these assumptions (especially for the explosions), more precise information is not currently available (e.g., local bulletins or reports from mining agencies). *Grant and Coyne* [1992] are currently assembling a database at CSS with this sort of information for this region, and we will retrain and retest our neural networks once these information become available. The origin information for these events, as produced by the *IMS*, are listed in Tables 10 and 11.

For each event, all vertical short period channel recordings (up to 25 array elements) from GERESS were used to construct 1–15 Hz incoherent beams (filter, rectify and stack). These were resampled, smoothed and windowed for P and S phases. Examples of these smoothed envelopes are shown in the bottom panel for each event in Figure 16. The shape of P-wave coda was represented by smoothed envelopes in the group velocity range 6.0–5.0 km/s. Figure 18 (top panel) shows the smoothed P-coda envelopes for all of the presumed earthquakes. Similarly, Figure 18 (middle panel) shows the P-coda envelopes for all of the presumed explosions. Visual inspection reveals a broad difference between the coda decay rate in the two populations, although there is much overlap. The fall-off of P-coda amplitude with time appears to be faster for the presumed explosion events (e.g., from mining areas in Poland) than it is for the presumed earthquakes to the south of GERESS. Figure 18 (bottom panel) is a superposition of all 61 envelopes used for neural network training.

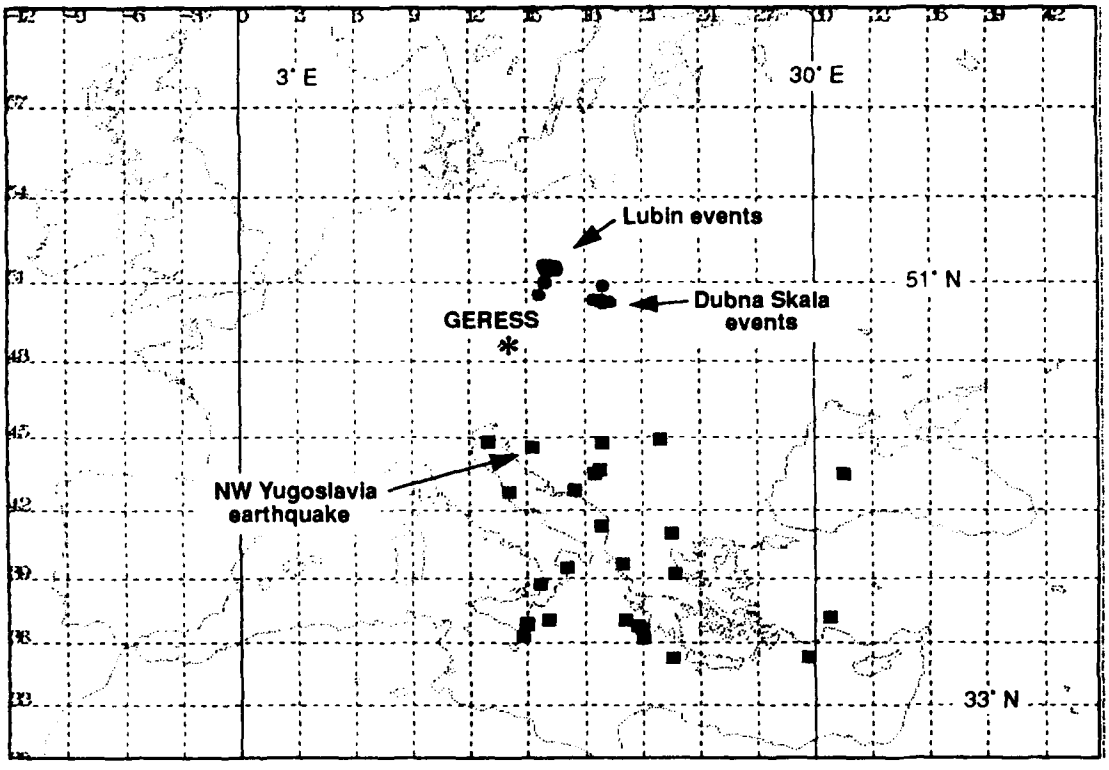

Figure 17. *61 events recorded at GERESS that are used for the event identification study. 35 of them are presumed to be explosions (solid circles) in mining areas (e.g., Lubin in Poland) and 26 are presumed to be earthquakes (solid squares) to the south of GERESS.*

Table 10. Bulletin of 26 Presumed Earthquakes Recorded at GERESS

orid[1]	Origin Time		Latitude	Longitude	Depth	M_L	nsta[2]	ndef[3]	Distance (km)
16201	91 04 04	19:03:41.358	43.66	18.84	0.0	3.0	3	4	695.9
19060	91 04 24	13:21:53.893	36.89	14.98	0.0	4.0	4	4	1330.2
20199	91 04 27	15:54:57.353	39.59	20.01	19.6	4.0	4	5	1141.7
20209	91 04 27	19:54:26.095	42.81	17.53	0.0	3.1	3	4	730.8
21392	91 04 29	21:38:12.061	43.50	18.56	0.0	3.2	4	5	699.8
30097	91 07 12	17:20:32.767	44.74	19.02	0.0	2.7	2	3	607.7
30933	91 07 17	00:22:22.603	36.65	21.02	0.0	3.7	4	5	1478.0
30934	91 07 17	20:05:46.099	36.76	20.80	0.0	3.8	4	5	1459.2
31346	91 07 21	01:56:27.366	35.20	22.60	0.0	4.0	4	5	1680.7
31384	91 07 21	15:03:31.674	37.05	20.11	0.0	3.9	3	3	1407.4
31399	91 07 23	08:40:50.255	42.73	14.07	0.0	3.1	3	4	678.1
31409	91 07 21	21:34:26.818	39.18	22.73	337.8	3.5	3	3	1290.3
31729	91 07 25	08:26:28.351	43.51	31.55	0.0	3.9	5	7	1491.8
32255	91 07 27	15:04:33.535	37.15	30.80	0.0	4.1	4	4	1893.9
32597	91 07 29	17:00:52.855	35.26	29.70	33.0	2.4	3	3	1996.7
33878	91 08 04	21:00:14.844	39.45	17.12	0.0	2.7	3	3	1077.2
34118	91 08 06	15:04:40.125	44.92	21.97	0.0	3.0	5	6	762.9
34999	91 08 15	04:58:57.212	40.93	22.56	0.0	4.4	4	5	1119.6
36561	91 08 28	00:03:37.872	44.57	15.34	0.0	3.5	2	5	489.4
36918	91 08 27	22:02:59.829	38.74	15.73	0.0	3.4	4	5	1132.5
38618	91 09 07	14:00:22.884	44.80	12.98	0.0	2.7	1	3	450.1
38789	91 09 08	19:45:16.211	41.28	18.94	33.0	3.8	5	7	934.1
41650	91 09 25	13:21:22.543	37.04	16.12	0.0	3.9	4	4	1327.3
41656	91 09 25	14:53:25.760	36.30	14.83	0.0	4.1	4	4	1398.1
41671	91 09 25	21:21:32.634	36.81	15.03	0.0	3.6	4	4	1342.1
41892	91 09 27	19:30:08.057	36.19	21.07	0.0	4.1	5	4	1529.8

1. Origin identification number.
2. The number of detecting stations.
3. The number of defining phases (number of phases used to locate the event).

Table 11. Bulletin of 35 Presumed Explosions Recorded at GERESS

orid[1]	Origin Time		Latitude	Longitude	Depth	M_L	nsta[2]	ndef[3]	Distance (km)
17185	91 04 07	08:35:12.681	51.64	15.96	0.0	2.3	4	8	351.9
17301	91 04 08	09:45:59.715	51.43	16.13	0.0	2.5	2	3	337.9
17658	91 04 11	19:31:13.357	51.59	16.52	0.0	2.4	4	6	367.5
17976	91 04 13	14:14:14.269	51.44	16.57	0.0	3.2	1	3	355.8
18742	91 04 18	04:37:39.429	51.63	15.87	0.0	2.8	3	5	348.0
19831	91 04 25	11:51:42.375	51.56	16.13	0.0	2.9	4	7	349.8
20297	91 04 30	03:40:36.346	51.55	16.33	0.0	3.0	4	5	356.2
20935	91 05 07	03:02:44.265	51.48	16.44	0.0	2.7	4	7	354.5
31002	91 07 20	03:23:35.140	51.54	16.08	0.0	3.1	2	5	347.0
31364	91 07 21	13:07:07.938	51.51	16.11	0.0	1.7	3	9	345.1
31388	91 07 21	17:10:50.781	51.43	16.06	0.0	1.9	3	6	335.7
31389	91 07 21	18:15:47.437	51.01	15.99	0.0	4.2	2	3	293.8
31416	91 07 21	22:50:41.171	51.60	16.22	0.0	1.8	4	8	357.3
31473	91 07 23	23:14:01.328	50.28	19.35	0.0	2.6	5	8	438.8
31610	91 07 24	03:17:45.260	51.64	16.02	0.0	2.7	5	8	354.2
32237	91 07 27	03:05:04.988	51.51	16.08	0.0	1.6	4	8	343.8
32252	91 07 27	14:05:59.267	51.55	16.08	0.0	1.7	4	8	347.3
32441	91 07 28	23:32:43.213	51.52	16.13	0.0	2.3	5	7	347.0
32757	91 07 30	15:03:53.429	50.34	18.88	0.0	3.7	2	5	409.4
32766	91 07 31	07:28:39.391	51.50	15.99	0.0	2.6	5	10	339.7
34139	91 08 07	12:16:20.669	51.47	16.28	0.0	2.8	3	5	346.8
34702	91 08 08	20:02:42.161	51.62	16.22	0.0	3.1	2	5	359.0
34970	91 08 14	21:51:06.307	50.34	18.50	0.0	2.7	2	4	384.9
35458	91 08 12	19:26:09.176	50.21	18.97	0.0	2.6	3	6	410.3
35595	91 08 20	10:29:10.244	50.53	15.66	0.0	4.2	1	3	236.4
36122	91 08 23	12:11:23.461	51.60	16.04	0.0	2.7	4	8	351.3
38301	91 09 06	11:32:53.503	51.56	16.18	0.0	2.8	5	8	352.0
38411	91 09 06	20:25:29.833	50.87	18.99	0.0	3.0	2	3	442.4
39452	91 09 13	02:23:19.482	51.57	16.36	0.0	2.1	5	9	360.1
39461	91 09 13	08:38:27.730	51.02	15.93	0.0	2.6	2	5	291.8
39700	91 09 11	16:24:20.401	51.59	16.06	0.0	2.3	5	9	350.5
41769	91 09 27	11:31:05.590	51.61	16.21	0.0	3.0	2	4	355.6
41791	91 09 27	16:05:04.348	51.59	16.05	0.0	2.3	5	10	347.9
41792	91 09 28	00:37:52.142	51.51	16.25	0.0	2.5	5	9	348.0
41796	91 09 28	04:00:14.608	50.31	18.78	0.0	2.4	2	4	400.9

1. Origin identification number.
2. The number of detecting stations.
3. The number of defining phases (number of phases used to locate the event).

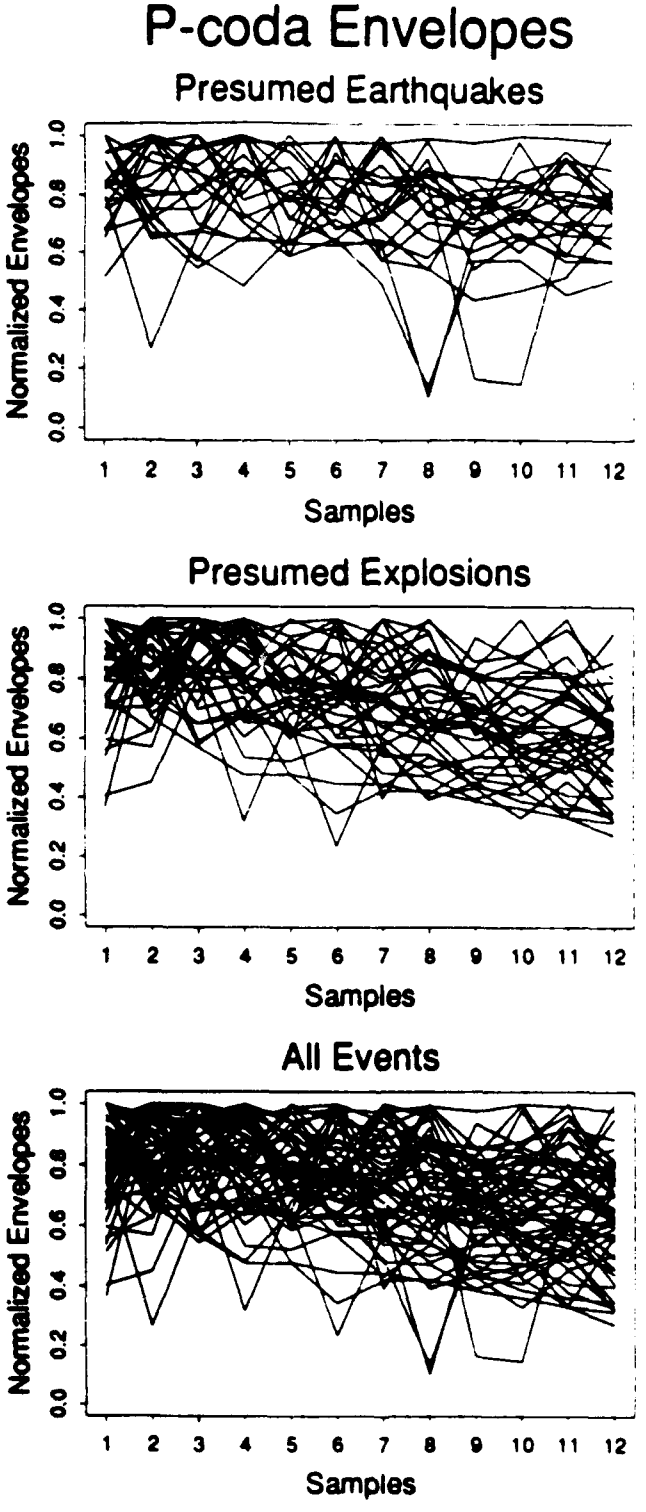

Figure 18. *The top panel is a superposition of all P-coda envelopes from 26 presumed earthquakes in the group velocity window 6.0–5.0 km/s. The middle panel shows the same from 35 presumed explosions, and the bottom panel is a superposition of all 61 envelopes. These envelopes were used for neural network simulation for regional seismic event identification.*

4.3 Experiment, Results and Observations

Figure 19 is a schematic diagram showing the architecture of the neural network method that we used for this study. The inputs to the neural network are the envelopes of regional seismic phases (ranging in number of samples from 6–30). The two output nodes represent the two event types. We added a middle layer of nodes; however, the level of accuracy was almost the same as using only two-layers (e.g., a single-layer perceptron). The results of our study are based on both types of networks. The number of nodes on the middle layer was determined empirically using the method described by *Patnaik and Sereno* [1991]. Our final 3-layer networks used 6 nodes in the middle layer.

There are not enough samples in our GERESS event set to split the data set into training and testing samples. Instead, we chose the *leave-one-out* approach to designing the classifier. In this method, the first sample is excluded and training is done with the remaining 60 samples. The first one is then used as a test sample. This is repeated 61 times, each time testing with the one left out. The score of percent correct classification is obtained by counting the number of times the testing succeeded. In this simplest case of *cross validation* technique, the estimated error rate is the number of wrong classifications divided by the total number of samples.

We experimented with both $P-$ and $S-$wave envelopes in various group velocity windows. We were careful to eliminate $S-P$ time differences in our windowing and resampling procedure. Nevertheless, differing source regions and propagation effects on the shape of the coda, if any, could not be removed. For example, close to perfect separation between earthquakes and explosions could be achieved if both P and S envelopes were used. This is probably caused by propagation effects, rather than source differences (e.g., many of the earthquakes had lower Lg amplitudes than the presumed explosions which is probably due to structural blockage along paths that cross the Alps).

Using only $P-$coda envelopes in the group velocity range 6.0–5.0 km/s, an overall identification accuracy of 77% was obtained for the GERESS data set (Table 12). 81% of the presumed explosions, and 73% of the presumed earthquakes were correctly identified. We conclude that the neural network classifier used the difference in coda decay rate for classifying these events. However, the uncertainty in *ground truth* prevents us from making any strong conclusions regarding the accuracy of the classifier. Further work is clearly necessary to develop this approach once a reliable *ground truth* data set becomes available [e.g., *Grant and Coyne*, 1992].

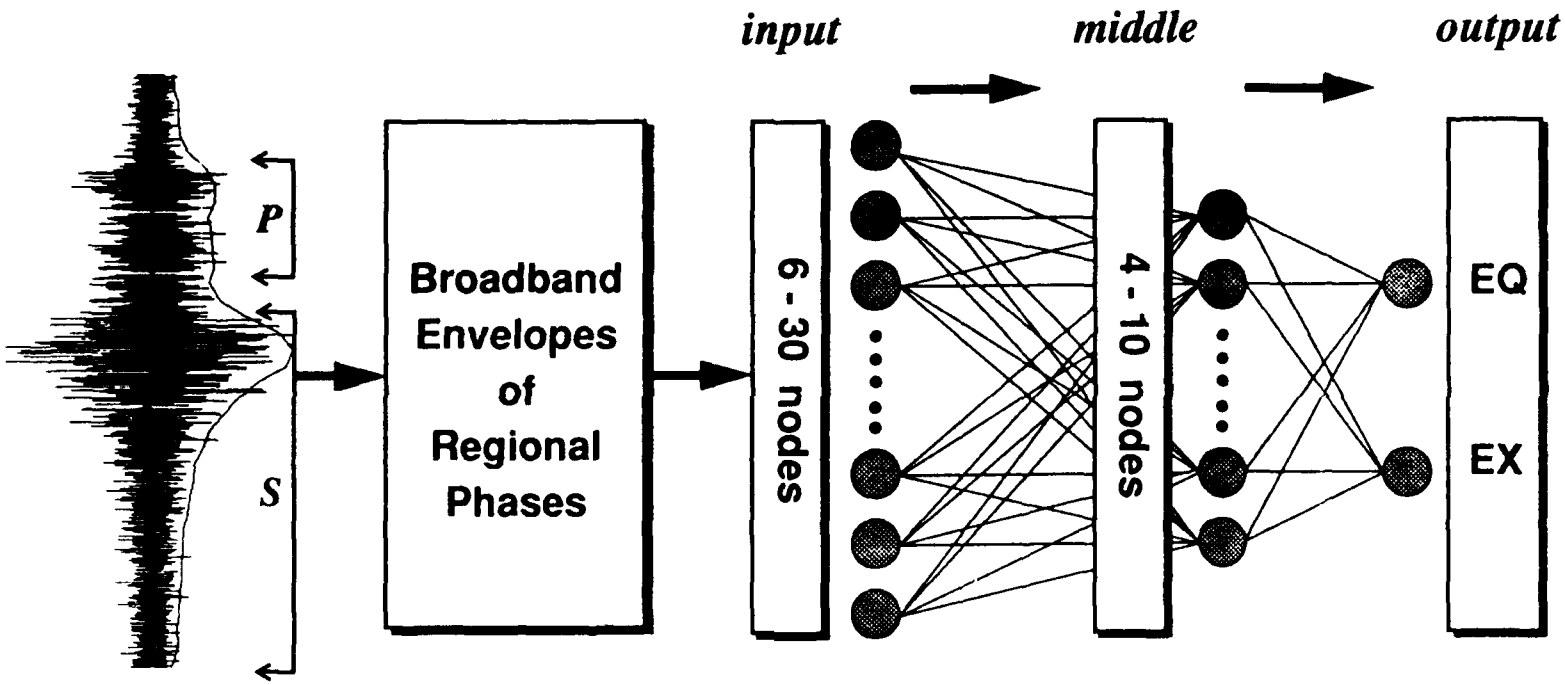

Figure 19. *Event Identification. Schematic diagram showing neural network architecture used for regional event identification.*

Table 12.

RESULTS

"Leave-one-out" Technique. Estimated Error Rate = 0.23

"GROUND TRUTH"	EXPL	QUAKE
EXPL	81%	19%
QUAKE	27%	73%

Overall event identification accuracy = 77%

5. CONCLUSIONS

We developed and implemented a neural network technique in *IMS* for automated initial identification of seismic phases (*P* or *S*) recorded by 3-component stations based on polarization and context data. The neural networks performed better than the current *IMS* rule-based system for interpreting data obtained from the 3-component IRIS/IDA stations in the former Soviet Union. The key advantages of the neural network approach to automated initial identification of seismic phases recorded by 3-component stations are:

- *Better performance than competing technologies.* The neural network consistently performed 3-6% better than both the current *IMS* rule-based system, and a linear multi-variate statistical technique [*Patnaik and Sereno*, 1991].

  The number of analyst events that were missed by automated processing is decreased by a factor of 2, by using neural networks for initial phase ID (about 10 events/week).

- *Extensibility.* The neural network approach is easily extended to include new features, which could be extremely difficult for a conventional rule-based system.
- *Adaptability.* The neural network is easily adapted to data from new stations. For example, the identification accuracy (*P* or *S*) is 75-85% without retraining (*e.g.*, using weights derived with data from a different station), and it is typically >95% after retraining with data from the same station. Enough data can be accumulated for retraining within a few weeks of continuous station operation, and training takes <30 minutes on a Sun Sparc Station.
- *Amenable to automated learning techniques.* The neural network approach is easily adapted to automated learning (e.g., training).

Under operational testing, the neural networks developed by MIT/Lincoln Laboratory for automated regional phase identification (e.g., *Pn, Pg, Sn, Lg,* and *Rg*), performed 3.3% better in identifying these phases than the current rule-based system in *IMS* for station processing. However, after network processing in the current system (where data from all stations are combined), the gain dropped to about 1.0%. It is possible that higher gains could be realized if network processing rules were modified to take advantage of the final phase confidence estimates from these neural networks.

Finally, our preliminary study on the application of neural networks to identify regional seismic events on the basis of their broadband envelope shape gave about 77% identification accuracy on data recorded at GERESS. The assumption of *ground truth* was that events clustered near the mining regions (e.g., Lubin in Poland) were explosions, and that the events to the south of GERESS were earthquakes. In general, the classifier utilized the coda decay rate which was lower for the earthquakes than it was for the explosions, although there was substantial overlap.

ACKNOWLEDGEMENTS

We thank Dr. Thomas Bache for suggesting us the problem of a comparative study of each 3-component array element using neural networks for initial phase identification.

Dr. Henry Swanger and Ms. Donna Williams analyzed the IRIS/IDA data used as the test database in this work. *Inference Corporation*, the software developer for *ESAL*, modified it to incorporate the two neural network modules reported in this work. Mrs. Christine Ferraro provided assistance with the graphics.

This research was funded by the Defense Advanced Research Projects Agency under contract number F19628–90–C–0156, and was monitored by Phillips Laboratory, Hanscom AFB.

REFERENCES

Bache, T., S. Bratt, H. Swanger, G. Beall, and F. Dashiell. "Knowledge-Based Interpretation of Seismic Data in the Intelligent Monitoring System", *Bull. Seism. Soc. Am.*, (*in preparation*), August, 1992.

Bache, T., S. Bratt, J. Wang, R. Fung, C. Kobryn, and J. Given. "The Intelligent Monitoring System", *Bull. Seism. Soc. Am.*, **80**, Part B, p.1833–1851, 1990.

Bennett, T., F. Scheimer, J., A. Campanella, and J. Murphy, "Seismic Discrimination of Rockbursts in Mines", in *Proceedings of the 14th Annual PL/DARPA Seismic Research Symposium*, **PL–TR–92–2210**, p.29–35, 16-18 September, 1992.

Bratt, S., G. Beall, H. Swanger, F. Dashiell, and T. Bache. "A Knowledge-Based System for Automatic Interpretation of Seismic Data to Associate Signals and Locate Events", *Quarterly Technical Report #8*, **SAIC–91/1281**, 1991.

Dowla, F.S., S. Taylor, and R. Anderson. "Seismic Discrimination with Artificial Neural Networks: Preliminary Results with Regional Spectral Data", *Bull. Seism. Soc. Am.*, **80**, p.1346–1373, 1990.

Dysart, P., and J. Pulli, "Regional Seismic Event Classification at the NORESS Array: Seismological Measurements and the Use of Trained Neural Networks", *Bull. Seism. Soc. Am.*, **80**, Part B, p.1910–1933, 1990.

Grant, L. and J. Coyne, "Ground–Truth Data for Seismic Discrimination Research" in *Proceedings of the 14th Annual PL/DARPA Seismic Research Symposium*, **PL–TR–92–2210**, p.139–145, 16-18 September, 1992.

Lacoss, R., R. Cunningham, S. Curtis, and M. Seibert. "Artificial Neural Networks for Seismic Data Interpretation", *Semiannual Tech. Rep.*, **ESD–TR–91–058**, Lincoln Laboratory, MIT, Lexington, MA, 30 November 1990, ADA239673.

Lacoss, R., S. Curtis, R. Cunningham, "Seismic Phase and Event Recognition Using Algorithms that Learn from Examples", in *Proceedings of the 14th Annual PL/DARPA Seismic Research Symposium*, **PL–TR–92–2210**, p.267–273, 16-18 September, 1992.

Patnaik, G.B. "Seismic Surface Wave Type Classification Using Artificial Neural Networks", *Geological Society of America Annual Meeting*, St. Louis–Missouri, GSA Abstracts With Programs, **21**, No. 6, 1989.

Patnaik, G.B., B.J. Mitchell and G.V. Rao, "Learned Classification of Seismic Events on Massively Parallel Networks", Paper presented at the Annual Meeting of the *Missouri Academy of Sciences*, St. Louis, Missouri, April 28, 1990.

Patnaik, G., and T. Sereno, "Neural Computing For Seismic Phase Identification", *Scientific Report No. 1 (Volume II)*, **PL–TR–92–2110(II)**, 1991. ADA252442.

Riviere-Barbier, F., A. Suteau-Henson, V. Ryaboy, and J. Carter, "Analysis of Three-Component Data from IRIS/IDA Stations in the USSR", *Bull. Seism. Soc. Am.*, **82**, No. 1, p.192–220, 1992.

Sereno, T., and G. Patnaik, "Data to test and evaluate the performance of neural network architectures for seismic signal discrimination", *Scientific Report No. 1 (Volume I)*, **PL–TR–92–2110(I)**, 1991. ADA254413.

Sereno, T., G. Patnaik, and M. Mortell, "Data to test and evaluate the performance of neural network architectures for seismic signal discrimination: Data sets #2–3", *Final Report (Volume I)*, **PL–TR–92–2218(I)**, 1992.

Su, F., K. Aki, and N.N. Biswas, "Discriminating Quarry Blasts from Earthquakes Using Coda Waves", *Bull. Seism. Soc. Am.*, **81**, No. 1, p.162–178, 1991.

Suteau-Henson, A. "Initial Phase Identification at the IRIS/IDA Stations in the USSR", in *Research at the Center for Seismic Studies*, Final Report (II), **PL–TR–92–2117(II)**, p.1–23, 1992a.

Suteau-Henson, A. "Confidence in Initial Phase Identification from Polarization at ARCESS and NORESS: a Comparison between Discriminant and Neural Network Methods", in *Research at the Center for Seismic Studies*, Final Report (II), **PL–TR–92–2117(II)**, p.25–46, 1992b.

Swanger, H., T. Sereno, D. Williams, and F. Ryall, "Eurasian Bulletin Produced by the Intelligent Monitoring System from Four Arrays and Six IRIS/IDA Stations", in *Proceedings of the 14th Annual PL/DARPA Seismic Research Symposium*, **PL–TR–92–2210**, p.408–414, 16-18 September, 1992.

Prof. Thomas Ahrens
Seismological Lab, 252-21
Division of Geological & Planetary Sciences
California Institute of Technology
Pasadena, CA 91125

Prof. Keiiti Aki
Center for Earth Sciences
University of Southern California
University Park
Los Angeles, CA 90089-0741

Prof. Shelton Alexander
Geosciences Department
403 Deike Building
The Pennsylvania State University
University Park, PA 16802

Dr. Ralph Alewine, III
DARPA/NMRO
3701 North Fairfax Drive
Arlington, VA 22203-1714

Prof. Charles B. Archambeau
CIRES
University of Colorado
Boulder, CO 80309

Dr. Thomas C. Bache, Jr.
Science Applications Int'l Corp.
10260 Campus Point Drive
San Diego, CA 92121 (2 copies)

Prof. Muawia Barazangi
Institute for the Study of the Continent
Cornell University
Ithaca, NY 14853

Dr. Jeff Barker
Department of Geological Sciences
State University of New York
at Binghamton
Vestal, NY 13901

Dr. Douglas R. Baumgardt
ENSCO, Inc
5400 Port Royal Road
Springfield, VA 22151-2388

Dr. Susan Beck
Department of Geosciences
Building #77
University of Arizona
Tuscon, AZ 85721

Dr. T.J. Bennett
S-CUBED
A Division of Maxwell Laboratories
11800 Sunrise Valley Drive, Suite 1212
Reston, VA 22091

Dr. Robert Blandford
AFTAC/TT, Center for Seismic Studies
1300 North 17th Street
Suite 1450
Arlington, VA 22209-2308

Dr. G.A. Bollinger
Department of Geological Sciences
Virginia Polytechnical Institute
21044 Derring Hall
Blacksburg, VA 24061

Dr. Stephen Bratt
Center for Seismic Studies
1300 North 17th Street
Suite 1450
Arlington, VA 22209-2308

Dr. Lawrence Burdick
Woodward-Clyde Consultants
566 El Dorado Street
Pasadena, CA 91109-3245

Dr. Robert Burridge
Schlumberger-Doll Research Center
Old Quarry Road
Ridgefield, CT 06877

Dr. Jerry Carter
Center for Seismic Studies
1300 North 17th Street
Suite 1450
Arlington, VA 22209-2308

Dr. Eric Chael
Division 9241
Sandia Laboratory
Albuquerque, NM 87185

Prof. Vernon F. Cormier
Department of Geology & Geophysics
U-45, Room 207
University of Connecticut
Storrs, CT 06268

Prof. Steven Day
Department of Geological Sciences
San Diego State University
San Diego, CA 92182

Marvin Denny
U.S. Department of Energy
Office of Arms Control
Washington, DC 20585

Dr. Zoltan Der
ENSCO, Inc.
5400 Port Royal Road
Springfield, VA 22151-2388

Prof. Adam Dziewonski
Hoffman Laboratory, Harvard University
Dept. of Earth Atmos. & Planetary Sciences
20 Oxford Street
Cambridge, MA 02138

Prof. John Ebel
Department of Geology & Geophysics
Boston College
Chestnut Hill, MA 02167

Eric Fielding
SNEE Hall
INSTOC
Cornell University
Ithaca, NY 14853

Dr. Mark D. Fisk
Mission Research Corporation
735 State Street
P.O. Drawer 719
Santa Barbara, CA 93102

Prof Stanley Flatte
Applied Sciences Building
University of California, Santa Cruz
Santa Cruz, CA 95064

Dr. John Foley
NER-Geo Sciences
1100 Crown Colony Drive
Quincy, MA 02169

Prof. Donald Forsyth
Department of Geological Sciences
Brown University
Providence, RI 02912

Dr. Art Frankel
U.S. Geological Survey
922 National Center
Reston, VA 22092

Dr. Cliff Frolich
Institute of Geophysics
8701 North Mopac
Austin, TX 78759

Dr. Holly Given
IGPP, A-025
Scripps Institute of Oceanography
University of California, San Diego
La Jolla, CA 92093

Dr. Jeffrey W. Given
SAIC
10260 Campus Point Drive
San Diego, CA 92121

Dr. Dale Glover
Defense Intelligence Agency
ATTN: ODT-1B
Washington, DC 20301

Dr. Indra Gupta
Teledyne Geotech
314 Montgomery Street
Alexanderia, VA 22314

Dan N. Hagedon
Pacific Northwest Laboratories
Battelle Boulevard
Richland, WA 99352

Dr. James Hannon
Lawrence Livermore National Laboratory
P.O. Box 808
L-205
Livermore, CA 94550

Dr. Roger Hansen
HQ AFTAC/TTR
Patrick AFB, FL 32925-6001

Prof. David G. Harkrider
Seismological Laboratory
Division of Geological & Planetary Sciences
California Institute of Technology
Pasadena, CA 91125

Prof. Danny Harvey
CIRES
University of Colorado
Boulder, CO 80309

Prof. Donald V. Helmberger
Seismological Laboratory
Division of Geological & Planetary Sciences
California Institute of Technology
Pasadena, CA 91125

Prof. Eugene Herrin
Institute for the Study of Earth and Man
Geophysical Laboratory
Southern Methodist University
Dallas, TX 75275

Prof. Robert B. Herrmann
Department of Earth & Atmospheric Sciences
St. Louis University
St. Louis, MO 63156

Prof. Lane R. Johnson
Seismographic Station
University of California
Berkeley, CA 94720

Prof. Thomas H. Jordan
Department of Earth, Atmospheric &
Planetary Sciences
Massachusetts Institute of Technology
Cambridge, MA 02139

Prof. Alan Kafka
Department of Geology & Geophysics
Boston College
Chestnut Hill, MA 02167

Robert C. Kemerait
ENSCO, Inc.
445 Pineda Court
Melbourne, FL 32940

Dr. Max Koontz
U.S. Dept. of Energy/DP 5
Forrestal Building
1000 Independence Avenue
Washington, DC 20585

Dr. Richard LaCoss
MIT Lincoln Laboratory, M-200B
P.O. Box 73
Lexington, MA 02173-0073

Dr. Fred K. Lamb
University of Illinois at Urbana-Champaign
Department of Physics
1110 West Green Street
Urbana, IL 61801

Prof. Charles A. Langston
Geosciences Department
403 Deike Building
The Pennsylvania State University
University Park, PA 16802

Jim Lawson, Chief Geophysicist
Oklahoma Geological Survey
Oklahoma Geophysical Observatory
P.O. Box 8
Leonard, OK 74043-0008

Prof. Thorne Lay
Institute of Tectonics
Earth Science Board
University of California, Santa Cruz
Santa Cruz, CA 95064

Dr. William Leith
U.S. Geological Survey
Mail Stop 928
Reston, VA 22092

Mr. James F. Lewkowicz
Phillips Laboratory/GPEH
Hanscom AFB, MA 01731-5000(2 copies)

Mr. Alfred Lieberman
ACDA/VI-OA State Department Building
Room 5726
320-21st Street, NW
Washington, DC 20451

Prof. L. Timothy Long
School of Geophysical Sciences
Georgia Institute of Technology
Atlanta, GA 30332

Dr. Randolph Martin, III
New England Research, Inc.
76 Olcott Drive
White River Junction, VT 05001

Dr. Robert Masse
Denver Federal Building
Box 25046, Mail Stop 967
Denver, CO 80225

Dr. Gary McCartor
Department of Physics
Southern Methodist University
Dallas, TX 75275

Prof. Thomas V. McEvilly
Seismographic Station
University of California
Berkeley, CA 94720

Dr. Art McGarr
U.S. Geological Survey
Mail Stop 977
U.S. Geological Survey
Menlo Park, CA 94025

Dr. Keith L. McLaughlin
S-CUBED
A Division of Maxwell Laboratory
P.O. Box 1620
La Jolla, CA 92038-1620

Stephen Miller & Dr. Alexander Florence
SRI International
333 Ravenswood Avenue
Box AF 116
Menlo Park, CA 94025-3493

Prof. Bernard Minster
IGPP, A-025
Scripps Institute of Oceanography
University of California, San Diego
La Jolla, CA 92093

Prof. Brian J. Mitchell
Department of Earth & Atmospheric Sciences
St. Louis University
St. Louis, MO 63156

Mr. Jack Murphy
S-CUBED
A Division of Maxwell Laboratory
11800 Sunrise Valley Drive, Suite 1212
Reston, VA 22091 (2 Copies)

Dr. Keith K. Nakanishi
Lawrence Livermore National Laboratory
L-025
P.O. Box 808
Livermore, CA 94550

Dr. Carl Newton
Los Alamos National Laboratory
P.O. Box 1663
Mail Stop C335, Group ESS-3
Los Alamos, NM 87545

Dr. Bao Nguyen
HQ AFTAC/TTR
Patrick AFB, FL 32925-6001

Prof. John A. Orcutt
IGPP, A-025
Scripps Institute of Oceanography
University of California, San Diego
La Jolla, CA 92093

Prof. Jeffrey Park
Kline Geology Laboratory
P.O. Box 6666
New Haven, CT 06511-8130

Dr. Howard Patton
Lawrence Livermore National Laboratory
L-025
P.O. Box 808
Livermore, CA 94550

Dr. Frank Pilotte
HQ AFTAC/TT
Patrick AFB, FL 32925-6001

Dr. Jay J. Pulli
Radix Systems, Inc.
2 Taft Court, Suite 203
Rockville, MD 20850

Dr. Robert Reinke
ATTN: FCTVTD
Field Command
Defense Nuclear Agency
Kirtland AFB, NM 87115

Prof. Paul G. Richards
Lamont-Doherty Geological Observatory
of Columbia University
Palisades, NY 10964

Mr. Wilmer Rivers
Teledyne Geotech
314 Montgomery Street
Alexandria, VA 22314

Dr. George Rothe
HQ AFTAC/TTR
Patrick AFB, FL 32925-6001

Dr. Alan S. Ryall, Jr.
DARPA/NMRO
3701 North Fairfax Drive
Arlington, VA 22209-1714

Dr. Richard Sailor
TASC, Inc.
55 Walkers Brook Drive
Reading, MA 01867

Prof. Charles G. Sammis
Center for Earth Sciences
University of Southern California
University Park
Los Angeles, CA 90089-0741

Prof. Christopher H. Scholz
Lamont-Doherty Geological Observatory
of Columbia University
Palisades, NY 10964

Dr. Susan Schwartz
Institute of Tectonics
1156 High Street
Santa Cruz, CA 95064

Secretary of the Air Force
(SAFRD)
Washington, DC 20330

Office of the Secretary of Defense
DDR&E
Washington, DC 20330

Thomas J. Sereno, Jr.
Science Application Int'l Corp.
10260 Campus Point Drive
San Diego, CA 92121

Dr. Michael Shore
Defense Nuclear Agency/SPSS
6801 Telegraph Road
Alexandria, VA 22310

Dr. Matthew Sibol
Virginia Tech
Seismological Observatory
4044 Derring Hall
Blacksburg, VA 24061-0420

Prof. David G. Simpson
IRIS, Inc.
1616 North Fort Myer Drive
Suite 1440
Arlington, VA 22209

Donald L. Springer
Lawrence Livermore National Laboratory
L-025
P.O. Box 808
Livermore, CA 94550

Dr. Jeffrey Stevens
S-CUBED
A Division of Maxwell Laboratory
P.O. Box 1620
La Jolla, CA 92038-1620

Lt. Col. Jim Stobie
ATTN: AFOSR/NL
Bolling AFB
Washington, DC 20332-6448

Prof. Brian Stump
Institute for the Study of Earth & Man
Geophysical Laboratory
Southern Methodist University
Dallas, TX 75275

Prof. Jeremiah Sullivan
University of Illinois at Urbana-Champaign
Department of Physics
1110 West Green Street
Urbana, IL 61801

Prof. L. Sykes
Lamont-Doherty Geological Observatory
of Columbia University
Palisades, NY 10964

Dr. David Taylor
ENSCO, Inc.
445 Pineda Court
Melbourne, FL 32940

Dr. Steven R. Taylor
Los Alamos National Laboratory
P.O. Box 1663
Mail Stop C335
Los Alamos, NM 87545

Prof. Clifford Thurber
University of Wisconsin-Madison
Department of Geology & Geophysics
1215 West Dayton Street
Madison, WS 53706

Prof. M. Nafi Toksoz
Earth Resources Lab
Massachusetts Institute of Technology
42 Carleton Street
Cambridge, MA 02142

Dr. Larry Turnbull
CIA-OSWR/NED
Washington, DC 20505

Dr. Gregory van der Vink
IRIS, Inc.
1616 North Fort Myer Drive
Suite 1440
Arlington, VA 22209

Dr. Karl Veith
EG&G
5211 Auth Road
Suite 240
Suitland, MD 20746

Prof. Terry C. Wallace
Department of Geosciences
Building #77
University of Arizona
Tuscon, AZ 85721

Dr. Thomas Weaver
Los Alamos National Laboratory
P.O. Box 1663
Mail Stop C335
Los Alamos, NM 87545

Dr. William Wortman
Mission Research Corporation
8560 Cinderbed Road
Suite 700
Newington, VA 22122

Prof. Francis T. Wu
Department of Geological Sciences
State University of New York
at Binghamton
Vestal, NY 13901

AFTAC/CA
(STINFO)
Patrick AFB, FL 32925-6001

DARPA/PM
3701 North Fairfax Drive
Arlington, VA 22203-1714

DARPA/RMO/RETRIEVAL
3701 North Fairfax Drive
Arlington, VA 22203-1714

DARPA/RMO/SECURITY OFFICE
3701 North Fairfax Drive
Arlington, VA 22203-1714

HQ DNA
ATTN: Technical Library
Washington, DC 20305

Defense Intelligence Agency
Directorate for Scientific & Technical Intelligence
ATTN: DTIB
Washington, DC 20340-6158

Defense Technical Information Center
Cameron Station
Alexandria, VA 22314 (2 Copies)

TACTEC
Battelle Memorial Institute
505 King Avenue
Columbus, OH 43201 (Final Report)

Phillips Laboratory
ATTN: XPG
Hanscom AFB, MA 01731-5000

Phillips Laboratory
ATTN: GPE
Hanscom AFB, MA 01731-5000

Phillips Laboratory
ATTN: TSML
Hanscom AFB, MA 01731-5000

Phillips Laboratory
ATTN: SUL
Kirtland, NM 87117 (2 copies)

Dr. Michel Bouchon
I.R.I.G.M.-B.P. 68
38402 St. Martin D'Heres
Cedex, FRANCE

Dr. Michel Campillo
Observatoire de Grenoble
I.R.I.G.M.-B.P. 53
38041 Grenoble, FRANCE

Dr. Kin Yip Chun
Geophysics Division
Physics Department
University of Toronto
Ontario, CANADA

Prof. Hans-Peter Harjes
Institute for Geophysic
Ruhr University/Bochum
P.O. Box 102148
4630 Bochum 1, GERMANY

Prof. Eystein Husebye
NTNF/NORSAR
P.O. Box 51
N-2007 Kjeller, NORWAY

David Jepsen
Acting Head, Nuclear Monitoring Section
Bureau of Mineral Resources
Geology and Geophysics
G.P.O. Box 378, Canberra, AUSTRALIA

Ms. Eva Johannisson
Senior Research Officer
National Defense Research Inst.
P.O. Box 27322
S-102 54 Stockholm, SWEDEN

Dr. Peter Marshall
Procurement Executive
Ministry of Defense
Blacknest, Brimpton
Reading FG7-FRS, UNITED KINGDOM

Dr. Bernard Massinon, Dr. Pierre Mechler
Societe Radiomana
27 rue Claude Bernard
75005 Paris, FRANCE (2 Copies)

Dr. Svein Mykkeltveit
NTNT/NORSAR
P.O. Box 51
N-2007 Kjeller, NORWAY (3 Copies)

Prof. Keith Priestley
University of Cambridge
Bullard Labs, Dept. of Earth Sciences
Madingley Rise, Madingley Road
Cambridge CB3 OEZ, ENGLAND

Dr. Jorg Schlittenhardt
Federal Institute for Geosciences & Nat'l Res.
Postfach 510153
D-3000 Hannover 51, GERMANY

Dr. Johannes Schweitzer
Institute of Geophysics
Ruhr University/Bochum
P.O. Box 1102148
4360 Bochum 1, GERMANY